
MISSOURI S&T

CENTER FOR TRANSPORTATION INFRASTRUCTURE AND SAFETY

# High-Strength Self-Consolidating Concrete Girders Subjected To Elevated Compressive Fiber Stresses

by

John J. Myers, Ph.D., P.E.
and
Jared E Brewe, Ph.D.

**A National University Transportation Center at Missouri University of Science and Technology**

## *Disclaimer*

The contents of this report reflect the views of the author(s), who are responsible for the facts and the accuracy of information presented herein. This document is disseminated under the sponsorship of the Department of Transportation, University Transportation Centers Program and the Center for Transportation Infrastructure and Safety NUTC program at the Missouri University of Science and Technology, in the interest of information exchange. The U.S. Government and Center for Transportation Infrastructure and Safety assumes no liability for the contents or use thereof.

**Technical Report Documentation Page**

| 1. Report No. | 2. Government Accession No. | 3. Recipient's Catalog No. |
|---|---|---|
| NUTC R209 | | |

| 4. Title and Subtitle | 5. Report Date |
|---|---|
| High-Strength Self-Consolidating Concrete Girders Subjected To Elevated Compressive Fiber Stresses | August 2009 |
| | 6. Performing Organization Code |

| 7. Author/s | 8. Performing Organization Report No. |
|---|---|
| John J. Myers, Ph.D., P.E. and Jared E Brewe, Ph.D. | 00018532 |

| 9. Performing Organization Name and Address | 10. Work Unit No. (TRAIS) |
|---|---|
| Center for Transportation Infrastructure and Safety/NUTC program<br>Missouri University of Science and Technology<br>220 Engineering Research Lab<br>Rolla, MO 65409 | 11. Contract or Grant No.<br>DTRT06-G-0014 |

| 12. Sponsoring Organization Name and Address | 13. Type of Report and Period Covered |
|---|---|
| U.S. Department of Transportation<br>Research and Innovative Technology Administration<br>1200 New Jersey Avenue, SE<br>Washington, DC 20590 | Final |
| | 14. Sponsoring Agency Code |

15. Supplementary Notes

16. Abstract

There are limited measurements documented in the literature related to long-term prestress losses in self consolidated concrete (SCC) members. Recorded test data has shown variations in mechanical property behavior of SCC compared to conventional HSC mixtures in the 8-12 ksi range. Over the past year, precast manufacturers such as Coreslab Structures, Inc., in Marshall, MO have experienced inconsistencies in camber behavior with SCC which may be attributed to mechanical property variations, but variation in stress may also be a contributing factor. Additionally, increasing the allowable fiber stress limit is desired for full utilization of materials and members, as long as structural performance is maintained. Furthermore, accurate prediction of time-dependant prestress losses is essential for determination of the effective prestress force, which effects serviceability prediction and structural performance. Further investigation is required.

| 17. Key Words | 18. Distribution Statement |
|---|---|
| SCC, prestressed concrete, bridges | No restrictions. This document is available to the public through the National Technical Information Service, Springfield, Virginia 22161. |

| 19. Security Classification (of this report) | 20. Security Classification (of this page) | 21. No. Of Pages | 22. Price |
|---|---|---|---|
| unclassified | unclassified | 67 | |

Form DOT F 1700.7 (8-72)

# HIGH-STRENGTH SELF-CONSOLIDATING CONCRETE GIRDERS SUBJECTED TO ELEVATED COMPRESSIVE FIBER STRESSES
# PART I: PRESTRESS LOSS AND CAMBER BEHAVIOR

**Jared E Brewe, Ph.D.** is an Associate II in Structural Engineering and Mechanics for CTLGroup in Skokie, IL, and a former graduate student in the Department of Civil, Architectural, and Environmental Engineering at Missouri University of Science and Technology in Rolla, MO

**John J. Myers, Ph.D., P.E.,** is an Associate Professor and Interim Center Director for the CTIS National University Transportation Center in the Department of Civil, Architectural, and Environmental Engineering at Missouri University of Science and Technology in Rolla, MO

## SYNOPSIS

The design of prestressed concrete members is restricted by the requirement that the extreme compressive fiber stress at midspan be less than 60% of the concrete compressive strength at release of prestressing. The purported purpose of this limit is to address serviceability performance, but it places unnecessary limits on the capability of the materials. For this research program, six prestressed girders were produced with high-strength self-consolidating concrete (HS-SCC) and subjected to elevated compressive fiber stress levels ranging between 65% and 84% of initial concrete compressive strength at release of prestressing. Time dependent concrete surface strains were measured using a mechanical strain gage, with a focus on drying creep behavior and its relationship to prestress losses. This work demonstrates that current AASHTO LRFD loss prediction methods developed for high-strength concrete overestimate losses on the order of 18%, whereas older methods developed for normal strength concrete produced more accurate results. Based on these results and other evidence, the authors suggest increasing the allowable compressive stress limit at any location to at least 70% of the initial concrete compressive strength at release of prestressing.

**KEYWORDS:** self-consolidating concrete, high-strength concrete, prestressed concrete, allowable release stresses, prestress transfer, modulus of elasticity.

# INTRODUCTION

The possibility of increasing the allowable compressive stresses at release of prestressing has recently garnered significant interest. Stress limits are imposed to ensure adequate serviceability performance and to prevent premature failure of materials. As engineers continue to push the envelope on span length and girder spacing to reduce costs, bridge girders are subjected to increasingly higher levels of stress under service loading. Increasing the allowable limits at release of prestressing would increase the amount of steel a given section can contain and reduce or eliminate the need for draping or debonding of strands resulting in improved plant safety. Further, this would allow faster turnaround for precast plants since prestressing could be released at lower concrete strengths. In addition, an increasing number of precast plants would like to reap the benefits of self-consolidating concrete (SCC), but they are reluctant to use this material because its behavior and its use has been rather limited in prestressing applications. Therefore, this investigation studied the prestress loss behavior and structural performance of prestressed concrete girders produced with high-strength self-consolidating concrete (HS-SCC) subjected to elevated compressive fiber stresses at release of prestressing.

## High-Strength Self-Consolidating Concrete (HS-SCC)

High-Strength Concrete (HSC) is now widely accepted by the prestressed/precast concrete industry. It has many advantages, including reduced material requirements resulting from the use of more compact sections. It also permits longer girder spans and increased girder spacing, thereby reducing material and total bridge costs. Recently, SCC has gained wider acceptance due its performance characteristics in the fresh state. It can eliminate the need for vibration, which reduces fabrication time and labor costs, and it has a reduced potential for segregation, voids, and surface defects. Due to these advantages, SCC is used increasingly in the precast industry since numerous studies have examined its mechanical properties for use in precast members.

With mix proportioning and the availability of new admixtures that increase the flowability, SCC can eliminate the need for vibration. Although the fresh properties of SCC are beneficial, the effect on hardened properties can be detrimental. Research has indicated that SCC has reduced

modulus of elasticity (MOE) values compared to conventional normal-strength or high-strength concretes[1-4]. This reduced MOE can be attributed to the lower coarse aggregate contents often specified to obtain the required rheological characteristics of SCC[1]. It is common for HSC mixes to use significantly more course aggregate than SCC mixes, resulting in higher MOE levels[5,6,7]. For prestressed concrete girders, the MOE has a significant impact on serviceability performance. Thus the use of SCC for longer members may require higher levels of prestressing force to address serviceability. Schindler et al.[8] studied a large range of SCC mixes for use in prestressed concrete applications. Their work demonstrated that the MOE at release age (18 hours) was lower for SCC than for the control mixtures with comparable compressive strengths, but that later age MOE results were similar.

Structural testing of full scale SCC girders was performed by Naito et al.[2] to determine the nominal strengths. These tests determined that SCC girders perform comparably to high early-strength concrete (HESC) girders produced with similar materials. The report noted that material properties of SCC outperformed current industry recommendations[2], but these conclusions applied only to the specific mix used in that project and further testing of other SCC mixes is needed. Erkmen et al.[3] measured the time-dependant behavior of an SCC prestressed girder and compared it to a conventional concrete girder. They found that the mechanical properties and prestress loss performance were comparable among the girders. Current prediction equations for MOE, transfer length, and prestress losses produced satisfactory results for both conventional concrete and SCC girders. Zia et al.[4] experienced less favorable rheological behavior of a trial SCC, but they observed similar material performance of SCC and conventional concrete. They tested full-scale girders up to the design service loads in flexure and found acceptable elastic behavior and full recovery after unloading.

**Allowable Stress Limits**

Currently, *AASHTO LRFD Bridge Design Specifications*[9] (hereafter called *AASHTO LRFD*) Article 5.9.4.1.1 limits the extreme fiber stress in compression to 60% of the concrete compressive strength ($0.6f_{ci}'$) immediately after prestress transfer. *ACI 318-08 Building Code Requirements for Structural Concrete*[10] (hereafter called *ACI 318*) Section 18.4.1 limits the extreme fiber stress in compression at midspan to $0.6f_{ci}'$, but it has been updated since the 2005

code cycle to permit $0.7f_{ci}'$ at the ends of the member. The *PCI Standard Design Practice*[11] recognizes these limits but refers to a study by Noppakunwijai et al.[12] demonstrating that they are conservative. The standard design practice states that "it has been common practice to allow compression up to $0.70f_{ci}'$." In addition to the compression limits, allowable tensile stress limits also exist for extreme tension fibers. The intent of these limits is to address serviceability, as noted in the *ACI 318*[10] commentary, by preventing excessive camber and deflections, and to control or prevent cracking. Further, compression limits appear to serve as an indirect means to ensure that crushing of concrete does not occur at prestress transfer[12].

In an open forum section of the *PCI Journal*, Huo and Tadros[13] attempt to evaluate the rationale behind allowable compressive stress limits. To demonstrate the effect of the limits, they analyzed a square cross-section subjected to concentric prestressing. Their analysis used both linear elastic analysis and non-linear material behavior. The amount of prestressing was gradually increased from 20 to 62 strands, and the resulting concrete and steel stress and strain were determined. The linear analysis resulted in failure at 45 strands, whereas the non-linear analysis predicted failure at 62 strands. To remain within the limit ($0.6f_{ci}'$), the linear analysis allows only 25 strands, and the non-linear analysis allows 26. Since this forum was only a discussion, no recommendations were made regarding increasing the allowable stresses, but reference was made to a 1996 *PCI Standard Design Practice* stating that no problems have been found with release stress up to $0.75f_{ci}'$.

As an alternative to checking stress limits, Noppakunwijai et al.[12] presented a procedure based on strength design. As opposed to analyzing the structure using the current working stress approach, they analyzed the prestressed beam as a non-prestressed reinforced concrete column subjected to axial compression and moment. This strength design method makes several assumptions consistent with reinforced concrete: plane sections remain plane, concrete has no tensile strength, the equivalent rectangular stress block for concrete, and ultimate concrete compressive strain is 0.003. With strength design, load factors and strength reduction factors are used to ensure safety. The authors rationalize the value of the factors by comparing them to other code specifications applicable to similar design situations. Maintaining strain compatibility and stress equilibrium, the authors provide equations that can be solved for several member

properties. The main limitation of this method is the rigorous procedure needed to solve the equations. The authors attempt to eliminate this issue by demonstrating that a commercially available computer program can determine a solution. They provide an empirical equation to determine the allowable compressive stress limit if the engineer continues using working stress design:

$$\left(0.6+\frac{y_b}{5h}\right)f'_{ci} \le 0.75\,f'_{ci}$$

where $y_b$ = the distance from the neutral axis to the bottom fiber of the section, $h$ = the height of the section, and $f_{ci}'$ = the compressive strength of concrete at release of prestressing. Their examples demonstrate that their approach can eliminate the need for draped or debonded strands typically used to control fiber stresses. They also show that the strength design approach requires lower concrete strengths at release of prestressing. To test the strength design approach, they fabricated two inverted tee specimens with cast-in-place composite topping to measure the creep losses due to increased fiber stresses. The results showed no negative impact of higher compressive fiber stresses on camber development.

Another aspect of increased compressive fiber stresses is the effect they may have on prestress losses. The force in the prestressing strands is reduced by losses associated with elastic shortening, shrinkage, and creep of concrete, and relaxation of steel. The losses that may be affected by increased stresses within the concrete member are elastic shortening and creep. To explore the effect of increased fiber stresses on HSC girders, Hale and Russell[14] measured the time-dependant prestress losses for 360 days and found that equations recently included in the *AASHTO LRFD*[9] predicted the losses to within 6%. Their results also supported an increase in the allowable compressive stress limits to $0.70f_{ci}'$.

The camber performance of girders subjected to higher fiber stresses is also of concern, since excessive or differential camber can cause constructability problems. To measure time-dependant camber development, Castro et al.[15] fabricated reduced scale specimens and subjected them to elevated concrete stresses, both in compression and tension. The specimens were representative of standard Texas U-beams, I-girders, and double-tee beams, and they had fiber stresses ranging from $0.46f_{ci}'$ to $0.91f_{ci}'$ in compression. The results indicated that increasing the

fiber stress level increases the camber, which should be expected since the section is subjected to increased axial load and moment. The higher release stresses resulted in higher rates of camber growth at early ages, which was underestimated by prediction methods. They also showed, however, that long-term camber response was acceptable and accurately predicted.

**Prestress Loss Predictions**

The design of prestressed concrete members requires accurate prediction of the force in the prestressing strands, which is reduced over time by prestress losses. Several methods are available for prestress loss prediction, each falling into one of three categories: total lump sum estimates, rational approximate methods, and detailed time-dependent analyses. Most of these methods are presented in the *AASHTO LRFD*[9], the *Precast/Prestressed Concrete Institute (PCI) Design Handbook*[11], and the *PCI Bridge Design Manual*[16]. Several methods representing each of these three categories are presented here.

The *AASHTO LRFD* Approximate Estimates Method (Section 5.9.5.3) and *PCI Design Handbook* Total Loss Method fall into the total lump sum estimate category. The *AASHTO LRFD* method uses a simple equation that results in a value for the total long-term prestress losses. The *PCI Design Handbook* states that total loss in prestressed members will range from about 25 to 50 ksi (172 to 345 MPa) for normal weight concrete members. Although these methods provide a good benchmark, more refined analyses improve the accuracy of the prediction.

The rational approximate methods determine the loss from shrinkage, creep, and relaxation separately. The methods falling into this category include the *AASHTO LRFD* Refined Estimates (Section 5.9.5.4) and the *PCI Design Handbook* method, which has been described by Zia et al.[17]. Recently, changes have been made to the design equations used in the *AASHTO LRFD* based upon recommendations from the *National Cooperative Highway Research Program (NCHRP) Report 496: Prestress Losses in Pretensioned High-Strength Concrete Bridge Girders*[18]. This project expanded previous design equations to account for the difference in material properties between normal strength concrete and HSC. Another advantage of these methods is the ability to use either the design parameters from prediction equations or parameters

measured on samples representative of the member. These parameters would typically include the concrete strength, modulus of elasticity, ultimate shrinkage strain, and ultimate creep coefficient.

Detailed time-dependent analyses produce the most accurate prediction of prestress losses, but they are not commonly used in design due to the complexity of determining those losses. This complexity stems from the need for specific material properties and calculation of incremental deformation history of the member. Some of these methods are presented and referenced in the *PCI Bridge Design Manual*[16].

Recently, several research projects have explored the long-term prestress losses, with many attempting to quantify the effect of HSC and SCC on these losses. The largest project was summarized in the *NCHRP Report 496*[18], and it prompted changes to the *AASHTO LRFD*. A few other projects are presented here in greater detail.

Erkmen et al.[3] examined time-dependent prestress losses in full-scale SCC girders and found similar results for both normal HSC and SCC girders. They also found that the *PCI Design Handbook* loss prediction methods produced results approximately 15% higher than measured values, but they noted that the results were reasonable and consistent between conventional concrete and SCC girders. Naito et al.[2] concluded that the *PCI Design Handbook* method overestimated the prestress losses in both SCC and HSC girders. At 28 days the effective prestress was 16% higher in the SCC girder and 13% higher in the HSC girder than the PCI estimates. Hale and Russell[14] studied the prestress loss behavior of girders subjected to increased fiber stresses. They concluded that the third edition of the *AASHTO LRFD*[9] overestimated the prestress losses by roughly 50%. They found that the *NCHRP Report 496*[18] equations predicted the losses to within an average of 6%. Their results also supported an increase in the allowable compressive stress to $0.70f_{ci}'$.

**Concrete Subjected to High Compressive Stresses**

When the allowable stresses are exceeded, concrete is subjected to higher sustained compressive stresses that may result in microcracking or increased creep. Pang[19] investigated the effect of

sustained compressive stresses greater than $0.60f_{ci}'$ on the compressive strength and MOE of HSC. At 1 day, concrete cylinders were loaded in uniaxial compression to stress levels of 60, 70, and 80% of the 1-day compressive strength. The loads were sustained until testing at 7, 28, 63, 90, or 180-days. During this time, creep and shrinkage measurements were taken to evaluate the creep performance under high sustained stresses. Results indicated that sustained stress of 0.60 to $0.70f_{ci}'$ had no adverse effect on compressive strength, but two specimens loaded to $0.80f_{ci}'$ did fail prematurely. Pang speculated that a slight eccentricity caused the failure of those specimens. The sustained stresses also increased the MOE of the specimens. Creep of sustained load specimens was acceptable and comparable to creep at lower stress levels.

In another study on sustained load strength, Iravani and MacGregor[20] found that HSC performed well under sustained stress levels over 70% of the average 56-day compressive strength. They found that as the compressive strength increased, the sustained load strength (i.e., the amount of sustained load that does not cause failure,) increased as well. They also found that loading the cylinder eccentrically, but within the elastic kern, further increases the sustained load strength. Short-term stress-strain tests showed that the ascending branch of the stress strain curve became steeper as compressive strength increased (i.e., MOE increased with increasing $f_c'$).

## RESEARCH PROGRAM

This research program explored the performance of prestressed concrete (PC) girders subjected to elevated compressive fiber stresses at release of prestressing. The program was divided into two phases: measurement of time-dependant prestress losses and quantification of structural performance. The first phase of study is presented here in Part I of a two-part paper series; the second phase, including flexural and shear testing of the girders, will be discussed in Part II.

This program cast six reduced scale prestressed concrete girders with targeted release stresses between 60% and 80% of the initial concrete compressive strength. Time-dependant prestress losses were measured at regular intervals for 196 days, then were subjected to load in structural testing to failure.

## Concrete Materials

The precast concrete supplier used a Missouri Department of Transportation (MoDOT) approved high strength SCC mix. This mix is used in everyday operations at the plant and for MoDOT projects requiring higher compressive strength SCC. The design target compressive stresses were 8 ksi (55 MPa) at release of prestressing and 10 ksi (69 MPa) at 28 days. All six girders were cast simultaneously from the same batch; thus material properties were consistent. The mixture proportions used for this project are presented in **Table 1**. For mechanical property testing, 4 in. x 8 in. (100 mm x 200mm) cylinders were cast and stored with the girders until test age. Compressive strength was tested at release and at 28 days; the modulus of elasticity (MOE) was determined at 28 days.

**Cementitious materials** – The mix contained an ASTM Type III Portland cement as a cementitious binder material. Although some high strength SCC mixes are designed to contain supplementary cementitious materials such as fly ash or silica fume, the mix typically used for MoDOT projects of this nature does not.

**Aggregates** – Typically SCC can be produced using standard concrete aggregates, as long as aggregate gradation is considered when developing the SCC mix design. To produce a mix with the rheological characteristics of SCC while avoiding segregation problems, a uniform gradation is typically employed to minimize the voids between the aggregates. For the mix used here, the course aggregate was a locally available crushed limestone with a maximum aggregate size of ¾ in. (19 mm) conforming to MoDOT Specifications[21] Section 1005 Gradation E. The fine aggregate was natural Missouri river sand conforming to MoDOT Specification Section 1005. The combination of these particle size distributions produced a gap graded mix with a lack of particles in a sieve range from the No. 4 sieve to ⅜ in. (9.5 mm). To fill the gaps and achieve a uniform gradation, crushed limestone chips with a maximum size of no more than ⅜ in. (9.5 mm) were used. The resulting combination of fine and coarse aggregates produced a well graded distribution resulting in a smaller volume of voids.

The mix proportions indicate that the total coarse aggregate fraction (¾ in. (19mm) Grade E plus ⅜ in. (9.5 mm) chips) was 34.9% by weight. Since the mechanical properties of concrete are tied

to the constituent materials, the compressive strength and MOE are closely tied to the coarse aggregate type and content[6]. Typical high-strength concrete mixes have on average 45% coarse aggregate content, and they typically incorporate hard, dense, angular aggregates with improved bond characteristics[5,6,7]. In the study presented by Schindler et al.[8] the average coarse aggregate fraction of SCC mixes was 43%, with a low of 38.5%. The mixes used by Naito et al.[2] had coarse aggregate contents of 47.1% and 40.7% by weight for the high-early strength concrete (HESC) and SCC mixes, respectively. Erkmen et al.[3] reported an average coarse aggregate content of 37.5%. These indicate that the coarse aggregate content used in the present study was below that normally found in most SCC mixes and could result in compressive strength and MOE reductions. An additional factor in concrete stiffness is the individual stiffness of the aggregates. The use of crushed dolomitic limestone aggregate is common throughout Missouri, and previous studies have produced strengths well above 10 ksi (69 MPa) with typical MOE values. Since crushed limestone is mined from quarries, different ledges (or stratum) can have different mechanical properties. The dolomitic limestone from the Cedar Valley formation, ledges 8 and 9, that was used in this study may have come from a softer ledge limestone, resulting in a reduced stiffness.

**Admixtures** – To achieve the rheological characteristics of SCC, a polycarboxalate-based high-range water reducer (HRWR) conforming to ASTM C 494[22] Type F was used. Since this mix was designed to imitate a standard MoDOT mix, a neutralized Vinsol resin-based air entraining admixture conforming to ASTM C 260[23] was used to achieve a typical specified air content of 6%.

## Girder Designs

The girders were designed using provisions from *AASHTO LRFD*[9], *ACI 318-05*[24] and the *PCI Design Handbook, Sixth Edition*[11]. The only provision that was disregarded was the compressive fiber stress limits; all other provisions, including allowable tension limits, were followed. For simplicity of fabrication, all six prestressed girders were cast simultaneously on the same prestressing bed. This simultaneous casting produced an identical prestressing layout and jacking level for every member designed to avoid variations in fabrication. A typical cross-section is shown in **Figure 1**, with cross-sectional properties for all girders shown in **Table 2**.

To achieve higher fiber stresses, the entire section width was reduced in ¼ in. (6.4 mm) increments, resulting in a reduced area and moment of inertia, which in turn resulted in greater strand eccentricity leading to the higher stresses. As indicated by the test results, the target compressive strength at release of prestressing was not achieved, resulting in higher compressive fiber stresses than anticipated. Thus the label used for each beam in the results and discussion below corresponds to the actual percentage of concrete fiber stress. Each girder was cast to a length of 15 ft (4.57 m) to ensure full development of prestressing for the girders designed for flexural testing.

The longitudinal reinforcement consisted of six ½ in. (12.7 mm) diameter, low-relaxation prestressing strands. All strands were straight and fully bonded to the concrete, and all had a manufacturer reported MOE of 28,500 ksi (197,000 MPa), conforming to ASTM A 416[25]. The strands were jacked to 75% of the ultimate strength by the precaster, resulting in an initial stress before any loss of 202.5 ksi (1396 MPa). Elongation measurements taken before and after jacking were used to determine the initial jacking stress.

**Instrumentation**

To estimate the magnitude of the prestress losses, concrete surface strains were measured using a detachable mechanical (DEMEC) strain gauge. These strains were measured from stainless steel DEMEC target points attached to the girders using commercially available metal/concrete epoxy. The DEMEC gauge has an 8 in. (200 mm) gauge length and calibrated to measure strain to an accuracy of $8.01 \times 10^{-6}$ in./in. (mm/mm).

The first target point was placed at approximately 3 in. (76.2 mm) from the jacking end, with points spaced every 8 in. (200 mm) thereafter along the entire length of the beam. At each end, an additional set of target points was placed at the midpoint of the first to second and second to third points from the end. An additional set was placed at midspan, with the midpoint of the gauge length exactly at midspan. This arrangement resulted in 25 sets of target points along the length of the beam at the three locations on the web. The points were placed at different depths on the cross-section to facilitate development of strain profiles and section curvature and to permit study of the strain distribution effect. Along the top of the section, only three sets were

used at each end and three sets at midspan since these locations were seen as most critical. A representation of DEMEC target point locations for half of the beam is shown in **Figure 2**. The critical locations for prestress loss determination were chosen at midspan and at the ends because this is the location where fiber stresses are typically calculated and checked. The points along the rest of the length were used to confirm the concrete strains and to determine transfer and development length.

As a reference, initial measurements were taken prior to release of prestressing. Immediately after prestress release, measurements were taken to capture the elastic strain in the member. Follow-up measurements were then taken at 1 day, 7 days, 14 days, 28 days, and every 28 days thereafter to monitor losses associated with creep and shrinkage of concrete. The difference between the initial reference and later readings was the resulting strain in the concrete between a given set of DEMEC target points. From these measured concrete surface strains, an average strain at the center of gravity of the prestressing strands was calculated. The prestress losses were determined by multiplying this average strain by the MOE of the prestressing strands.

Camber measurements were also taken to model the development over time. These measurements were obtained by suspending a thin piano wire between two fixed points mounted at each end of the girder and measuring the distance between the wire and the top of the girder using a ruler with 1/32 in. (0.79 mm) increments. The difference between the average of the end measurements and the measurement at midspan represented the camber of the girder.

## EXPERIMENTAL RESULTS

### Fresh Concrete Properties

At concrete placement, fresh concrete properties were measured following applicable ASTM standards and the PCI SCC Guidelines[26]; test results are shown in **Table 3**. The SCC slump flow was evaluated according to ASTM C 1611[27] using the inverted-slump-cone spread test with a result of 27 in. (68.5 cm). This value was slightly above the targeted range of 22 – 26 in. (56 – 66 cm) but it did not result in segregation of the mix. The concrete temperature, air content, and

density were typical of normal prestressed concrete members for MoDOT projects requiring the use of SCC.

**Hardened Concrete Properties**

Concrete mechanical properties were tested at release of prestressing (3 days), 28 days, 56 days, and at test age (243 days). Concrete compressive strength was tested in accordance with ASTM C 39[28], and the MOE was tested according to ASTM C 469[29]. Concrete compressive strength at 3 days was found to be 7088 psi (48.8 MPa). The 28-day compressive strength was 9026 psi (62.2 MPa), with an MOE of 4635 ksi (31940 MPa). The concrete strength at 243 days was found to be 8210 psi (56.6 MPa) with an MOE of 4175 ksi (28785 MPa). **Table 4** presents the average, coefficient of variation, and number of concrete cylinder tests at 28, 56, and 243 days. A reduction in cylinder compressive strength of nearly 10% between 28 days and 243 days can only be explained by the improper calibration of testing machines. The 28 and 56 day tests were performed on a Forney compression machine, and the 243 day tests were split, with three tests on the Forney machine and three on a Tinius-Olsen testing machine. Between the 56 and 243 day tests, the Forney machine was recalibrated, which likely caused the change in strength measurements. Since the target strength was not reached, the values of the compressive fiber stresses exceeded values specified in the design as shown in **Table 2**.

The MOE at both 28 and 243 days was significantly lower than anticipated, which affected the prestress loss behavior of the members. The MOE predicted according to *AASHTO LRFD* Article 5.4.2.4 is presented in **Table 4,** along with the ratio of measured to predicted values. As discussed above, a reduced value was expected due to the low coarse aggregate fraction, but this value was even lower than anticipated. Discussions with the precaster, suggest that the combination of low coarse aggregate contents and a softer layer of limestone at the quarry led to the reduced MOE values.

Due to testing limitations at the precast plant, the MOE was not determined at release of prestressing. Rather, it was estimated from a proportional relationship of the square root of the compressive strength. A factor determined from the relationship between test age strength and MOE values was used to calculate the MOE from the release strength. This method is similar to

the correction factor method typically used for prediction of the MOE at specific plants or laboratories to account for the source of the aggregate.

**Prestress Loss Predictions**

As mentioned above, several methods of prestress loss prediction are in use. This project used the *AASHTO LRFD* Fourth Edition[9] Refined Estimates method, the *PCI Design Handbook*[11] method, and the *AASHTO LRFD* Third Edition[30] to compare predicted to measured values. The third edition of the *AASHTO LRFD* was chosen since the method was developed for normal strength concrete and thus facilitates comparison to the fourth edition published in 2007, which was modified to account for higher strength concrete. Less common methods of prestress loss prediction are not discussed here.

Prestress losses were predicted at two stages: immediately after release, accounting for the elastic shortening of the member, and at 196 days, to match the measurement schedule and thus account for long term losses due to shrinkage and creep. As mentioned above, the relaxation of steel does not correspond to a change in strain. Since such relaxation is not measured, that loss is ignored in the following calculations. For design purposes, however, it would have been considered in determination of the total prestress losses. The notation used in the following equations can be found at the end of the paper.

The following equation is used to determine elastic shortening losses using both *AASHTO LRFD* methods:

$$\Delta f_{pES} = \frac{E_{ps}}{E_{ci}} f_{cgp}$$

where $\Delta f_{pES}$ = the prestress loss due to elastic shortening, $E_{ps}$ = the modulus of elasticity of the prestressing strands, $E_{ci}$ = the modulus of elasticity of concrete at release of prestressing, and $f_{cgp}$ = the concrete stress at the center of gravity of prestressing. This method requires iteration since the value of the prestressing force is used to determine $f_{cgp}$, which is then reduced by the calculated losses. The commentary of the *AASHTO LRFD* offers a direct solution that can be used to avoid iteration. The equation in the *PCI Design Handbook* is similar to that presented

above; however, it assumes the prestressing force to be 90% of the initial prestressing force and requires no iteration.

The determination of long-term losses requires the prediction or estimation of the long-term properties of the concrete. Older methods used in the *PCI Design Handbook* and the third edition of the *AASHTO LRFD* were developed for normal strength concrete, and their calculations involve several assumptions. The newer method uses fewer assumptions to increase accuracy, but some assumptions remain.

The fourth edition of the *AASHTO LRFD* guides the designer through the process of predicting shrinkage and creep of the concrete; it then provides equations for determination of the associated losses. The equations for determining shrinkage are:

$$\varepsilon_{sh} = 480\times10^{-6}\,\gamma_{sh}$$

$$\gamma_{sh} = k_{td}\,k_s\,k_{hs}\,k_f$$

where $\varepsilon_{sh}$ = the concrete shrinkage strain with the following factors calculated as shown:

Time-Development: $$k_{td} = \frac{t}{61-4\,f'_{ci}+t}$$

Humidity (for shrinkage): $$k_{hs} = 2.00 - 0.0143RH$$

Size: $$k_s = \frac{1064-94V/S}{735}$$

Concrete Strength: $$k_f = \frac{5}{1+\,f'_{ci}}$$

where *RH* = the relative humidity, and *V/S* = the volume-to-surface area ratio. The ultimate shrinkage is assumed to be 480 microstrain. Although this value should hold true for most HSC, more shrinkage can be expected here because the coarse aggregate fraction of the current SCC mix was significantly lower, as previously shown. Earlier editions of the *AASHTO LRFD* used an ultimate shrinkage strain of 560 microstrain for accelerated curing and 510 microstrain for moist curing, but the equations used to determine the influential factors were different.

The equation for determining concrete creep is:

$$\psi_b = 1.9 k_s k_{hc} k_f k_{td} t_i^{-0.118}$$

where $\psi_b$ = the creep coefficient. The majority of factors included here are the same as those used for shrinkage prediction, with the addition of the following:

Humidity (for creep): $k_{hs} = 1.56 - 0.008RH$

In this equation, the ultimate creep coefficient is assumed to be 1.9. Since creep is proportional to applied stress and varies for different concrete mixtures, the assumed value of this coefficient affects the accuracy of the predictions.

A transformed section coefficient, $K_{id}$, is used to account for time-dependent interaction between concrete and bonded steel, which is determined with the following equation:

$$K_{id} = \frac{1}{1 + \frac{E_{ps}}{E_{ci}} \frac{A_{ps}}{A_g} \left( 1 + \frac{A_g e_{pg}^2}{I_g} \right) [1 + 0.7\psi_b]}$$

where $A_g$ = the gross area of section, $A_{ps}$ = the area of prestressing steel, $e_{pg}$ = the eccentricity of prestressing steel, and $I_g$ = the gross section moment of inertia. Therefore, the losses from shrinkage, $\Delta f_{pSH}$, and creep, $\Delta f_{pCR}$,are determined from the following equations:

$$\Delta f_{pSH} = \varepsilon_{sh} E_{ps} K_{id}$$

$$\Delta f_{pCR} = \frac{E_{ps}}{E_{ci}} f_{cgp} \psi_b K_{id} = \Delta f_{pES} \psi_b K_{id}$$

The use of improved equations to determine the specific material properties used in the loss prediction equations can be expected to improve accuracy. Testing for the specific material properties used in the prediction equations should also improve accuracy by eliminating assumptions.

The *PCI Design Handbook* method does not require that the designer determine the concrete material properties, and it provides the following equation for the determination of loss due to concrete shrinkage:

$$\Delta f_{pSH} = \left(8.2 \times 10^{-6}\right) E_{ps} \left(1 - 0.06 V/S\right) \left(100 - RH\right)$$

Some of the same variables used in the *AASHTO LRFD* methods are used here to account for member size and relative humidity. Similarly, the equation for determination of losses from concrete creep:

$$\Delta f_{pCR} = 2.0\frac{E_{ps}}{E_c}\left(f_{cir} - f_{cds}\right)$$

where $f_{cir}$ = the concrete stress at the center of gravity of the steel immediately after transfer and $f_{cds}$ = the concrete stress at the center of gravity of the steel due to service dead loads. The assumptions are evident in both of these equations. The assumed ultimate shrinkage strain is not indicated, but the previous method accounts for a larger number of variables. The same simplification holds for the creep coefficient, but an assumption of 2.0 is used.

The third edition of *AASHTO LRFD* used straightforward equations for the determination of long-term prestress losses. The equations for shrinkage and creep of concrete are:

$$\Delta f_{pSH} = 10.7 - 0.15RH$$

$$\Delta f_{pCR} = 12.0\, f_{cgp} - 7.0\, f_{cds}$$

where $f_{cgp}$ = the concrete stress at the center of gravity of the prestressing. The simplicity of these equations does not allow the designer much control over specific material properties, but the results are reasonably accurate for some members. The concrete mixture proportions used in the present study resembled a traditional, normal strength concrete mix rather than an HSC mix, and these equations were developed for normal strength concrete. Therefore, they may more accurately predict the prestress losses.

**Prestress Loss Behavior**

The time-dependant material properties used for the prestress loss predictions were those found in *AASHTO LRFD*. Ideally, actual measurement of ultimate shrinkage strain and the creep coefficient would improve the accuracy of the predictions. In the work by Schindler et al.[8], the 112-day drying shrinkage was found to be on the same order of magnitude as that of the control mixtures. Naito et al.[2] found that the girder produced using SCC experienced less creep and shrinkage than the HESC girder.

The development of prestress losses over time is presented in **Table 5**. These losses were calculated from three measurements at midspan. These measurements were averaged to the

center of gravity of the steel; therefore the resulting loss was determined from a total of nine measurements. As expected, the members with a greater fiber stress level exhibited an increasing amount of prestress loss due to elastic shortening. Beam 79 represents the only abnormality in the trend. The cause of this irregularity is unclear since the beams were cast from the same batch and the as-cast dimensions were as designed. The following sections will further show that the girder camber was closely predicted.

The time-dependent prestress losses exhibit the same trend as the elastic losses, with an increase in magnitude of loss as fiber stresses increase. The same irregularity emerges with respect to Beam 79, but in addition Beam 68 appears to have undergone greater long-term prestress loss. For comparison, the last line in **Table 5** presents the ratio of total long-term losses at 196 days to the elastic losses. Excluding Beam 68, with increasing fiber stresses at release, a larger percentage of the total prestress loss appears to result from elastic shortening.

**Figure 3** is a visual representation of the reduction in prestressing force over time due to the losses presented in **Table 5**. The initial prestressing force was 202.5 ksi (1396 MPa). As noted above, the results were similar for all beams except Beam 79, which exhibited larger values at both elastic and long-term, and Beam 68 which showed greater long-term losses. Additionally, this plot demonstrates that the majority of prestress losses occurred within the first six months as the stresses began to level out after 140 days.

**Table 6** compares measured and predicted losses. The measured elastic losses are underestimated in nearly every instance, with varying degrees of accuracy for each prediction method. The AASHTO methods are analogous; therefore, both prediction methods produce comparable results with similar underestimation. Since the only properties used in calculations at this stage are the geometric properties and the elastic modulus of each material, these results were expected to be the most accurate.

Results were mixed for the prediction of long-term losses. The 2007 *AASHTO* LRFD refined method underestimated the prestress losses for all beams by an average of 18%. The PCI method overestimated for all beams by an average of 21%. The third edition of *AASHTO LRFD*

produced an average overestimation of 10%. Each of the individual methods produced mixed results across the range of fiber stress levels.

**Prediction of Camber**

The eccentricity of the prestressing typically causes concrete girders to deflect upward, an effect known as camber. At release, two factors influence the deformation: camber from prestressing and deflection from dead load. The upward camber due to prestressing was calculated from Equation 18 using the MOE of concrete and the transformed section moment of inertia calculated at release of prestressing.

$$\Delta_{ps} = \frac{A_{ps} f_{pt} e_{ps} L^2}{8 E_{ci} I_{tr}}$$

where $f_{pt}$ = the stress in the prestressing immediately after transfer, $I_{tr}$ = the transformed section moment of inertia at release of prestressing, and $L$ = the member length.

In addition, downward deflection due to dead loads was calculated using:

$$\Delta_{d} = \frac{5 M_{d} L^2}{48 E_{ci} I_{t}}$$

where $I_t$ = transformed section moment of inertia at long-term and $M_d$ = member dead load moment. The sum of these values equals the total deformation (camber or displacement) at release of prestressing.

The long-term deformation must account for the previous causes of deformation as well as additional downward deflection due to the loss of prestress**,** which uses long term material and sectional properties, is determined from:

$$\Delta_{loss} = \frac{A_{ps} \Delta f_{pLT} e_{ps} L^2}{8 E_{c} I_{t}}$$

where $E_c$ = modulus of elasticity of concrete at long-term and $\Delta f_{pLT}$ = total long-term prestress losses.

The remaining source of deformation was the creep of concrete due to the sustained load of prestressing. Two methods can account for this deformation: an effective elastic modulus can be

calculated to account for the effects of creep, or a creep coefficient can be multiplied by the initial deformation to determine the additional creep deformation. The prediction of prestress loss includes the calculation of the creep coefficient; therefore, the additional deformation due to concrete creep was easily determined using:

$$\Delta_{cr} = (\Delta_{ps} - \Delta_d)\psi_b \quad (21)$$

The total deformation equals the sum of the results of each deflection equation.

**Camber Results**

The measured and predicted camber versus time for each girder is presented in **Figures 4** through **9**. The predictions agree considerably with actual measurements. The use of actual concrete properties eliminated errors stemming from incorrect material properties assumptions. The largest differences occurred at early ages, between release and 50 days. Accurate prediction of camber is essential within this time frame since typical bridge girders are placed on the structure and composite decks formed and cast at this age.

## CONCLUSIONS

The following conclusions can be drawn from the results of this research:

1. Prediction of elastic shortening losses for all beams was less accurate than anticipated. The accuracy was expected to improve because the properties used are less variable at early ages, but the results show otherwise.
2. Prestress loss predictions for HS-SCC girders with compressive fiber stresses well above $0.6f_{ci}'$ vary significantly according to the prediction methods. Older methods developed for normal strength concrete overestimate prestress loss, whereas the newer methods developed for HSC underestimate the losses compared to measured values.
3. Accurate prediction of material properties will affect the 2007 *AASHTO LRFD* model. Proper measurement and testing of ultimate shrinkage strains and creep coefficients would improve accuracy.
4. As suggested by data shown on the last line in **Table 5**, higher fiber stress levels result in a larger proportion of the total long-term losses resulting from elastic shortening.

5. Camber performance for all specimens can be predicted with acceptable accuracy. Early differences are due to the development of material properties over time.
6. As indicated by previous work, increasing the fiber stress level to at least $0.70f_{ci}'$ appears feasible.

Although the results presented here indicate older methods produce more accurate predictions, the authors believe that the 2007 *AASHTO LRFD* method would produce superior results for the majority of projects because this method uses improved equations with fewer assumptions. However, a database on HS-SCC would facilitate development of modifiers and further improve the accuracy of predictions.

## ACKNOWLEDGEMENTS

The authors would like to acknowledge the financial support of Coreslab Structures, Inc. in Marshall, Missouri and that of the Center for Transportation Infrastructure and Safety (CTIS) at the Missouri University of Science and Technology (formerly the University of Missouri-Rolla). Thanks are also due to the engineers and personnel at Coreslab Structures, Inc., for their contributions during planning and production. The technician and staff support from the Center for Infrastructure Engineering Studies (CIES) and Department of Civil, Architectural, and Environmental Engineering at the Missouri University of Science and Technology has also provided much appreciated assistance.

## REFERENCES

1. Bonen, D.; and Shah, S.; "The Effect of Formulation of the Properties of Self-Consolidating Concrete," *Concrete Science and Engineering: A Tribute to Arnon Bentur*, Proceedings of the International RILEM Symposium, K. Kovler, J. Marchand, S. Mindess, and J. Weiss, eds., RILEM Publications, France, 2004, pp. 43-56
2. Naito, C.J.; Parent, G.; and Brunn, G.; "Performance of Bulb-Tee Girders Made with Self-Consolidating Concrete," *PCI Journal*, V. 51, No. 6, November–December 2006, pp. 72-85

3. Erkmen, B.; Shield, C.K.; and French, C.E.; "Time-Dependent Behavior of Full-Scale Self-Consolidating Concrete Precast Prestressed Girders," *Self-Consolidating Concrete for Precast Prestressed Applications (ACI SP-247)*, A. Schindler, D. Trejo, and R. Barnes, eds., American Concrete Institute, Farmington Hills, MI (2007) pp. 139-153
4. Zia, P.; Nuez, R.A.; Mata, L.A.; and Dwairi, H.M.; "Implementation of Self-Consolidating Concrete for Prestressed Concrete Girders," *Proceedings of the 7th International Symposium of High-Strength/High-Performance Concrete (ACI SP-228)*, H.G. Russell, ed., American Concrete Institute, Farmington Hills, MI (2005) pp. 297-316
5. Cook, J. E., "10,000 psi," Concrete International, V. 11, No. 10, October 1989, pp. 67–75
6. Huo, X.S.; Al-Omaishi, N.; and Tadros, M.K.; "Creep, Shrinkage, and Modulus of Elasticity of High-Performance Concrete," *ACI Materials Journal*, V. 98, No. 6, November-December 2001, pp. 440-449
7. Myers, J.J. (1998). "Production and Quality Control of High Performance Concrete in Texas Bridge Structures," Dissertation, University of Texas – Austin
8. Schindler, A.K.; Barnes, R.W.; Roberts, J.B.; and Rodriguez, S.; "Properties of Self-Consolidating Concrete for Prestressed Members," *ACI Materials Journal*, V. 104, No. 1, January-February 2007, pp. 53-61
9. American Association of State Highway and Transportation Officials, *AASHTO-LRFD Bridge Design Specifications*, Fourth Edition, Washington, DC (2007)
10. American Concrete Institute (ACI 318-08), *Building Code Requirements for Structural Concrete*, American Concrete Institute, Farmington Hills, MI (2008)
11. Precast/Prestressed Concrete Institute, *PCI Design Handbook, Precast and Prestressed Concrete*, Sixth Edition, Chicago, IL (2004)
12. Noppakunwijai, P.; Tadros, M.K.; Ma, Z.; and Mast, R.F.; "Strength Design of Pretensioned Flexural Concrete Members at Prestress Transfer," *PCI Journal*, V. 46, No. 1, January-February 2001, pp. 34-52
13. Huo, X.; and Tadros, M.K.; "Allowable Compressive Strength of Concrete at Prestress Release," *PCI Journal*, Open Forum Section, V. 42, No. 1, January-February 1997, pp. 95-99

14. Hale, W.M.; and Russell, B.W.; "Effect of Allowable Compressive Stress at Release on Prestress Losses and on the Performance on Precast, Prestressed Concrete Bridge Girders," *PCI Journal*, V. 51, No. 2, March–April 2006, pp. 14-25
15. Castro, A.; Kreger, M.E.; Bayrak, O.; Breen, J.E.; and Wood, S.L.; "Allowable Design Release Stresses for Pretensioned Concrete Beams," *Center for Transportation Research Report 0-4086-2*, The University of Texas at Austin, August 2004, 127 pp.
16. Precast/Prestressed Concrete Institute, *PCI Bridge Design Manual*, First Edition, Chicago, IL (2000)
17. Zia, P.; Preston, H.K.; Scott, N.L.; and Workman, E.B.; "Estimating Prestress Losses," *Concrete International*, V. 1, No. 6, June 1979, pp. 32-38
18. Tadros, M.K.; Al-Omaishi, N.; Seguirant, S.J.; and Gallt, J.G.; "Prestress Losses in Pretensioned High–Strength Concrete Bridge Girders," *National Cooperative Highway Research Program Report 496*, TRB, National Research Council, Washington DC (2003)
19. Pang, J.P.; *Allowable Compressive Stresses for Prestressed Concrete*, Master's Thesis, University of Oklahoma, 1997
20. Iravani, S; and MacGregor, J.G.; "Sustained Load Strength and Short-Term Strain Behavior of High-Strength Concrete," *ACI Materials Journal*, V. 95, No. 5, September-October 1998, pp. 636-647
21. Missouri Department of Transportation, *2004 Missouri Standard Specifications for Highway Construction*
22. ASTM C 494, Standard Specification for Chemical Admixtures for Concrete, ASTM International, West Conshohocken, PA
23. ASTM C 260, Standard Specification for Air-Entraining Admixtures for Concrete, ASTM International, West Conshohocken, PA
24. American Concrete Institute (ACI 318-05), *Building Code Requirements for Structural Concrete*, American Concrete Institute, Farmington Hills, MI (2005)
25. ASTM A 416, Standard Specification for Steel Strand, Uncoated Seven-Wire for Prestressed Concrete, ASTM International, West Conshohocken, PA
26. PCI Interim SCC Guidelines FAST Team, *Interim Guidelines for the Use of Self-Consolidating Concrete in Precast/Prestressed Concrete Institute Member Plants*, PCI Report TR-6-03, Precast/Prestressed Concrete Institute, Chicago, IL, April 2003

27. ASTM C 1611, Standard Test Method for Slump Flow of Self-Consolidating Concrete, ASTM International, West Conshohocken, PA
28. ASTM C 39, Standard Test Method for Compressive Strength of Cylindrical Concrete Specimens, ASTM International, West Conshohocken, PA
29. ASTM C 469, Standard Test Method for Static Modulus of Elasticity and Poisson's Ratio of Concrete in Compression, ASTM International, West Conshohocken, PA
30. American Association of State Highway and Transportation Officials, *AASHTO-LRFD Bridge Design Specifications*, Third Edition, Washington, DC, Interim 2005

## NOTATION

$A_g$ = gross area of section
$A_{ps}$ = area of prestressing steel
$e_{pg}$ = eccentricity of prestressing steel
$E_{ps}$ = modulus of elasticity of prestressing strands
$E_{ci}$ = modulus of elasticity of concrete at release
$f_{cir}$ = concrete stress at center of gravity of steel immediately after transfer
$f_{cgp}$ = concrete stress at center of gravity of prestressing
$f_{cds}$ = concrete stress at center of gravity of steel due to service dead loads
$f_{ci}'$ = concrete compressive strength at release of prestressing
$f_{pt}$ = stress in prestressing immediately after transfer
$h$ = height of section
$I_g$ = gross section moment of inertia
$I_t$ = transformed section moment of inertia at long-term
$I_{tr}$ = transformed section moment of inertia at release
$k_f$ = effect of concrete strength factor
$k_{hc}$ = humidity factor for creep
$k_{hs}$ = humidity factor for shrinkage
$k_s$ = effect of volume-to-surface area ratio factor
$k_{td}$ = time development factor
$K_{id}$ = transformed section coefficient

1 $I_{tr}$ = transformed section moment of inertia at release
2 $M_d$ = member dead load moment
3 $RH$ = relative humidity
4 $V/S$ = volume-to-surface area ratio
5 $y_b$ = distance from neutral axis to bottom fiber of section
6 $\Delta_{cr}$ = camber due to creep.
7 $\Delta_d$ = deflection due to member dead load
8 $\Delta_{loss}$ = deflection due to loss of prestressing
9 $\Delta_{ps}$ = camber due to prestressing
10 $\Delta f_{pCR}$ = prestress loss due to creep of concrete
11 $\Delta f_{pES}$ = prestress loss due to elastic shortening
12 $\Delta f_{pLT}$ = total long-term prestress losses
13 $\Delta f_{pSH}$ = prestress loss due to shrinkage of concrete
14 $\varepsilon_{sh}$ = concrete shrinkage strain
15 $\psi_b$ = girder creep coefficient

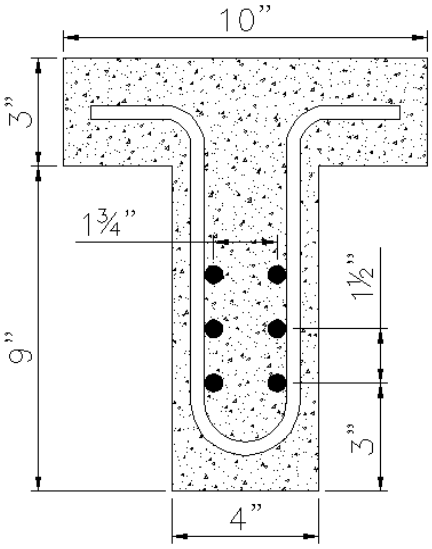


**Figure 1** – Typical Cross-Section

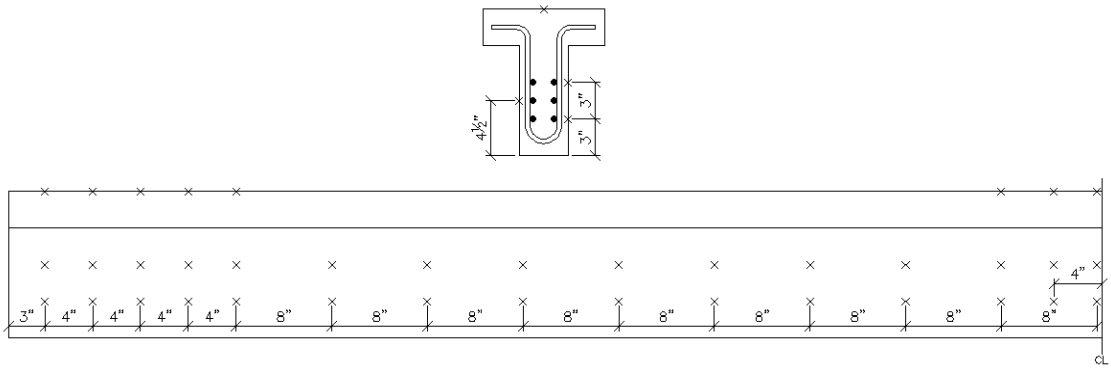


**Figure 2** – Location of DEMEC Target Points

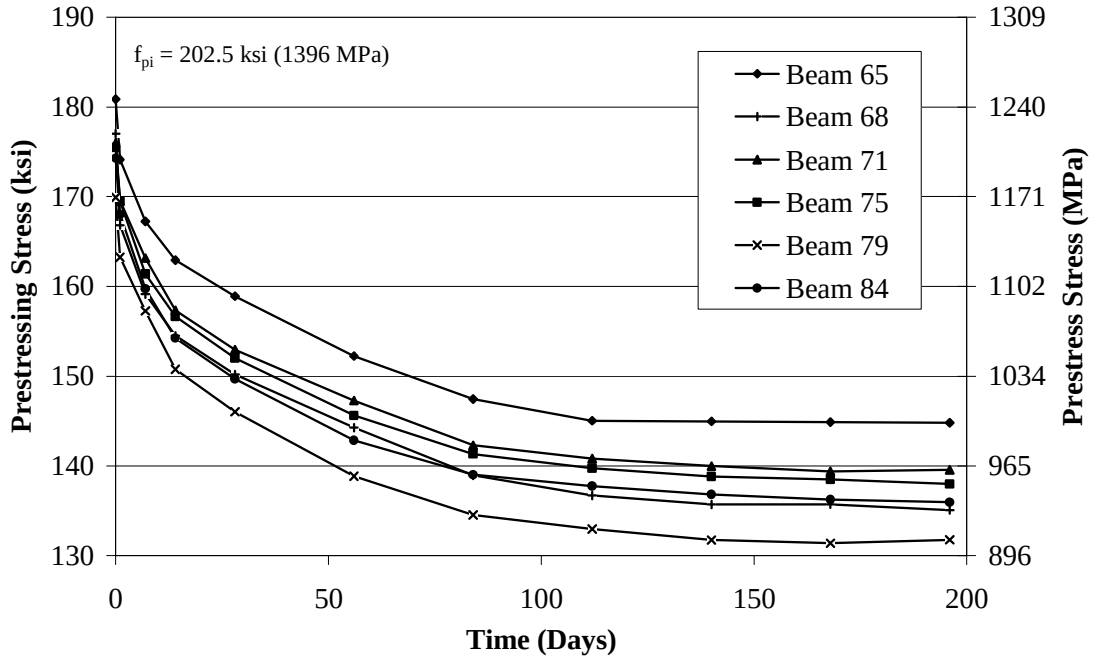


**Figure 3** – Loss of Prestressing Stress over Time

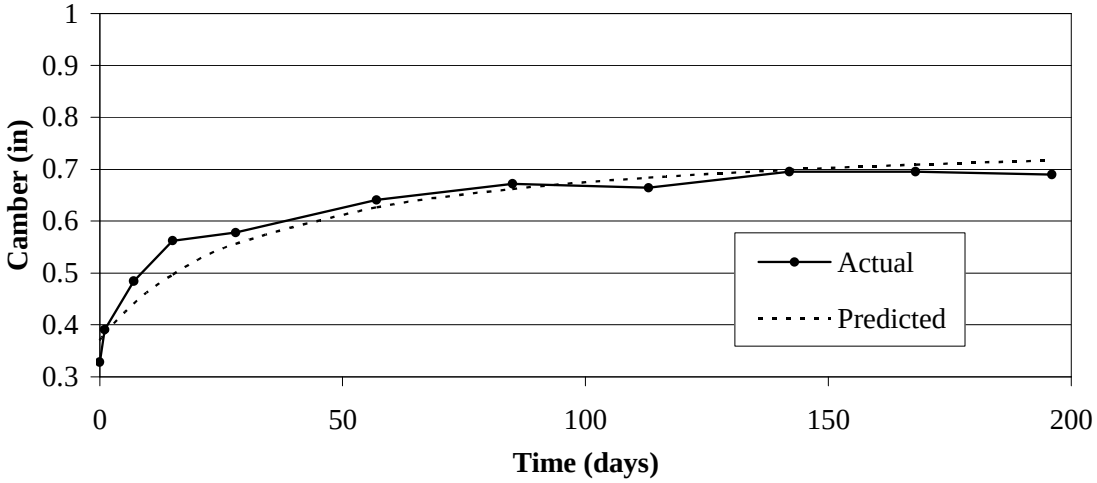


**Figure 4 –** Camber Development for Beam 65

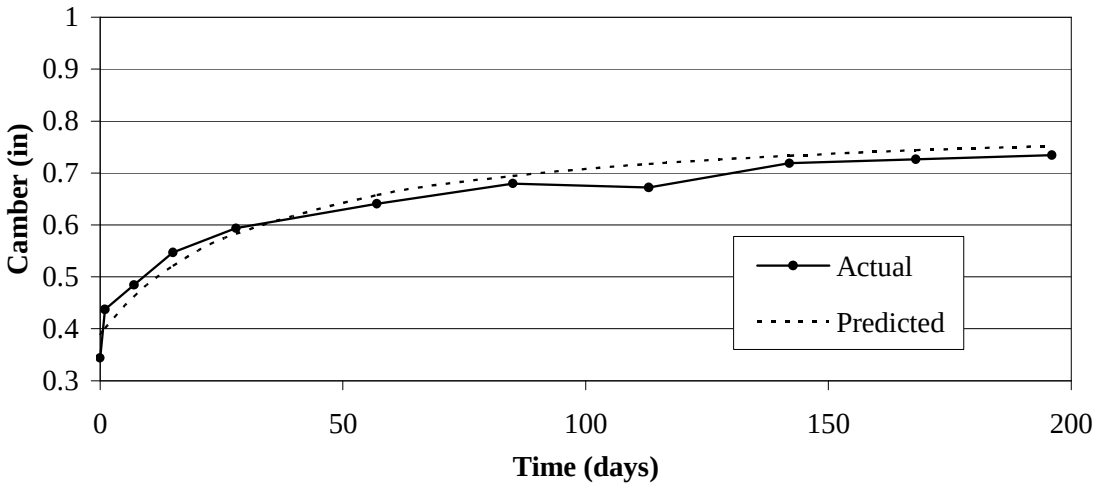


**Figure 5** – Camber Development for Beam 68

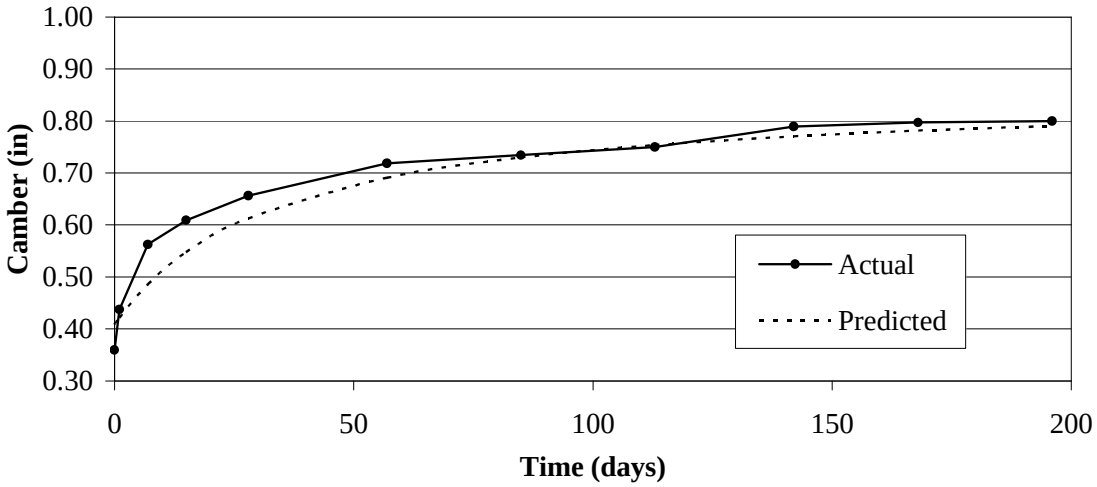


**Figure 6** – Camber Development for Beam 71

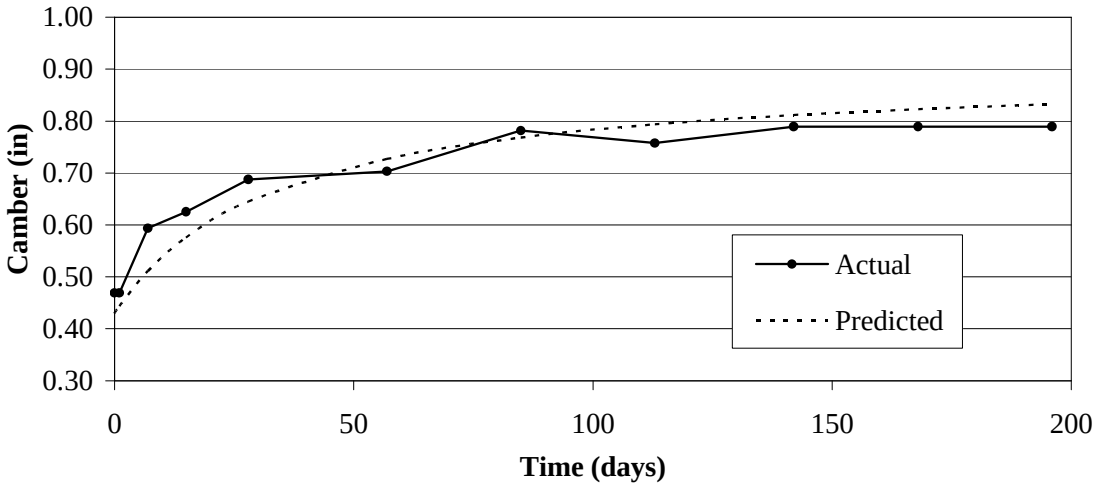


**Figure 7** – Camber Development for Beam 75

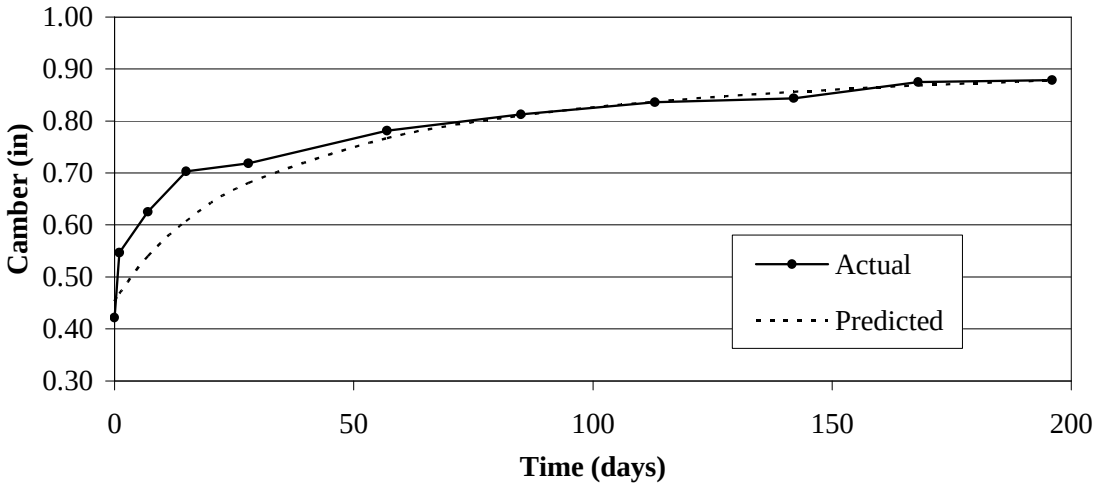


**Figure 8** – Camber Development for Beam 79

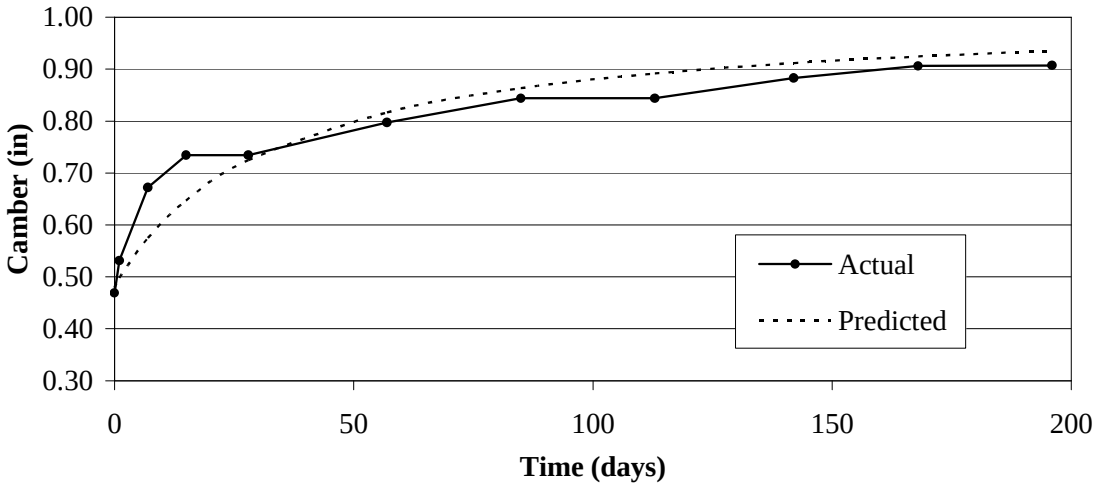


**Figure 9** – Camber Development for Beam 84

**Table 1** – Mixture Proportions

| Mix Constituent Materials | | Description |
|---|---|---|
| **Cement** | 777 lb/yd$^3$ | ASTM Type III Portland Cement |
| **Coarse Aggregate** | 889 lb/yd$^3$ | Crushed Limestone – ¾ inch MAS |
| **Intermediate Aggregate** | 460 lb/yd$^3$ | Crushed Limestone Chips - ⅜ inch MAS |
| **Fine Aggregate** | 1419 lb/yd$^3$ | ASTM C 33 - Natural River Sand |
| **HRWR** | 90 oz/yd$^3$ | ASTM C 494 Type F - Polycarboxylate |
| **Air Entrainment** | 12 oz/yd$^3$ | ASTM C 260 – Neutralized Vinsol Resin |
| **Water-Cementitious Ratio** | 0.369 | – |

Note: 1 lb/yd$^3$ = 0.5933 kg/m$^3$, 1 inch = 25.4 mm, 1 oz/yd$^3$ = 38.69 mL/m$^3$

**Table 2** - Beam Cross-Sectional Properties

| Girder Designation | B-84 | B-79 | B-75 | B-71 | B-68 | B-65 |
|---|---|---|---|---|---|---|
| **Target Stress Level (% of $f`_{ci}$)** | 80 | 75 | 71 | 68 | 64 | 60 |
| **Actual Stress Level (% of $f`_{ci}$)** | 84 | 79 | 75 | 71 | 68 | 65 |
| **Gross Area, $A_g$ (in$^2$)** | 66 | 69 | 72 | 75 | 78 | 81 |
| **Gross Moment of Inertia, $I_g$ (in$^4$)** | 855 | 895 | 935 | 975 | 1014 | 1053 |
| **Distance from CGC to Top Fiber, $y_t$ (in)** | 4.77 | 4.83 | 4.88 | 4.92 | 4.96 | 5.00 |
| **Distance from CGC to Bottom Fiber, $y_b$ (in)** | 7.23 | 7.17 | 7.13 | 7.08 | 7.04 | 7.00 |
| **Strand Eccentricity, $e_p$ (in)** | 2.73 | 2.67 | 2.63 | 2.58 | 2.54 | 2.50 |
| **Distance from Top Fiber to CGS, $d_p$ (in)** | 7.50 | | | | | |

Note: CGC = center of gravity of concrete, CGS = center of gravity of steel; 1 in.= 25.4 mm

**Table 3** – Fresh Concrete Properties

| Fresh Concrete Properties | Test Result |
|---|---|
| **Spread (in)** | 27 |
| **Concrete Temperature (°F)** | 70 |
| **Air Content (%)** | 6.8 |
| **Unit Weight (lb/ft$^3$)** | 138 |

Note:1 in.= 25.4 mm, °C = (5/9)(°F-32), 1 lb/ft$^3$ = 16.02 kg/m$^3$

**Table 4** – Hardened Concrete Properties

| Test Age | 28 days | 56 days | 243 days |
|---|---|---|---|
| **Average Compressive Strength (psi)** | 9026 | 9024 | 8210 |
| **Coefficient of Variation** | 0.80% | 1.41% | 1.94% |
| **Number of Compression Tests** | 3 | 3 | 6 |
| **Average MOE (ksi)** | 4635 | – | 4175 |
| **Predicted MOE[1] (ksi)** | 5082 | – | 4847 |
| **Ratio of Measured to Predicted MOE** | 0.912 | – | 0.861 |

Note: 1 ksi = 6.89 MPa, 1 – According to *AASHTO LRFD 5.4.2.4*

**Table 5** – Measured versus Predicted Prestress Losses

| Average Measured Prestress Loss at CGS (ksi) | | | | | | | |
|---|---|---|---|---|---|---|---|
| **Designation** | | **84** | **79** | **75** | **71** | **68** | **65** |
| **Beam Age (Days)** | Elastic | 28.2 | 32.6 | 27.0 | 26.5 | 25.5 | 21.6 |
| | 1 | 34.5 | 39.3 | 33.0 | 32.9 | 35.7 | 28.4 |
| | 7 | 42.7 | 45.2 | 41.1 | 39.3 | 43.4 | 35.3 |
| | 14 | 48.3 | 51.7 | 45.8 | 45.2 | 48.0 | 39.6 |
| | 28 | 52.8 | 56.5 | 50.5 | 49.5 | 52.3 | 43.6 |
| | 56 | 59.7 | 63.7 | 56.9 | 55.2 | 58.3 | 50.3 |
| | 84 | 63.5 | 68.0 | 61.2 | 60.2 | 63.5 | 55.0 |
| | 112 | 64.8 | 69.6 | 62.8 | 61.7 | 65.8 | 57.5 |
| | 140 | 65.7 | 70.8 | 63.7 | 62.5 | 66.8 | 57.5 |
| | 168 | 66.3 | 71.1 | 64.0 | 63.1 | 66.8 | 57.6 |
| | 196 | 66.5 | 70.7 | 64.5 | 62.9 | 67.4 | 57.7 |
| $\Delta f_{p196} / \Delta f_{pES}$ | | **2.36** | **2.17** | **2.39** | **2.37** | **2.65** | **2.67** |

Note: Losses do not include relaxation of steel, 1 ksi = 6.89 MPa

**Table 6** Comparison Between Measured and Predicted Losses (with percent error)

| **Designation** | **84** | **79** | **75** | **71** | **68** | **65** |
|---|---|---|---|---|---|---|
| **Elastic Losses (ksi)** | | | | | | |
| Measured | 28.2 | 32.6 | 27.0 | 26.5 | 25.5 | 21.6 |
| *AASHTO LRFD* | 27.7 | 26.3 | 25.1 | 23.9 | 22.9 | 21.9 |
| | -2% | -19% | -7% | -10% | -10% | 1% |
| *PCI* | 29.0 | 27.3 | 25.8 | 24.4 | 23.2 | 22.1 |
| | 3% | -16% | -5% | -8% | -9% | 2% |
| **Total Losses at 196 days (ksi)** | | | | | | |
| Measured | 66.5 | 70.7 | 64.5 | 62.9 | 67.4 | 57.7 |
| *AASHTO LRFD 4th Ed.* | 58.7 | 56.3 | 54.2 | 52.2 | 50.3 | 48.6 |
| | -12% | -20% | -16% | -17% | -25% | -16% |
| *PCI* | 88.8 | 84.0 | 79.7 | 75.9 | 72.4 | 69.2 |
| | 33% | 19% | 24% | 21% | 7% | 20% |
| *AASHTO LRFD 3rd Ed.* | 79.3 | 75.6 | 72.3 | 69.3 | 66.5 | 64.0 |
| | 19% | 7% | 12% | 10% | -1% | 11% |

Note: Losses do not include relaxation of steel, 1 ksi = 6.89 MPa

# HIGH-STRENGTH SELF-CONSOLIDATING CONCRETE GIRDERS SUBJECTED TO ELEVATED COMPRESSIVE FIBER STRESSES
## PART II: STRUCTURAL BEHAVIOR

**Jared E Brewe, Ph.D.** is an Associate II in Structural Engineering and Mechanics for CTLGroup in Skokie, IL, and a former graduate student in the Department of Civil, Architectural, and Environmental Engineering at Missouri University of Science and Technology in Rolla, MO

**John J. Myers, Ph.D., P.E.,** is an Associate Professor and Interim Center Director for the CTIS National University Transportation Center in the Department of Civil, Architectural, and Environmental Engineering at Missouri University of Science and Technology in Rolla, MO

## SYNOPSIS

The design of prestressed concrete members is restricted by the requirement that the extreme compressive fiber stress at midspan be less than 60% of the concrete compressive strength at release of prestressing. The purported purpose of this limit is to provide serviceability performance, but it places unnecessary limits on the capability of the materials. For this research program, six prestressed girders were produced with high-strength self-consolidating concrete and subjected to elevated compressive fiber stress levels ranging between 65% and 84% of initial concrete compressive strength at release of prestressing. Part I of this series analyzed time-dependent prestress losses and camber behavior and compared these to the results of typical prediction methods. This second part examines the flexural and shear behavior of the same girders. The results of structural testing indicated little reduction in flexural performance of girders subjected to elevated stress levels, but further testing of the shear behavior is needed to reduce variability in the results. The results reported here suggest that an increase in the allowable compressive stress limit at any location is feasible up to at least 70% of the initial concrete compressive strength at release of prestressing.

KEYWORDS: self-consolidating concrete, high-strength concrete, prestressed concrete, allowable release stresses, prestress transfer, modulus of elasticity

# INTRODUCTION

Two goals prompt reconsideration of allowable compressive stress limits for concrete members at release of prestressing: to improve safety by eliminating the need for harping of strands, and to increase plant productivity by allowing the release of prestressing at lower concrete strengths. Part I[1] of this series evaluated allowable compressive stress limits and reviewed their implications for the use of high-strength self-consolidating concrete (HS-SCC) in prestressed concrete members. These issues have attracted significant interest due to their importance for the prestressed concrete industry. Additional background information on this research program is presented in Part I of this series.

## Concrete Subjected to High Compressive Stresses

For ultimate strength, flexural steel reinforcement is located below the neutral axis of the prestressed member. At release of prestressing, the applied prestressing force compresses the bottom fiber, resulting in negative bending. Under service loading, the beam is subjected to positive bending, creating tension on the bottom fiber. If the net result of prestressing and service loading exceeds the tensile strength of the concrete, cracks develop. Typically under service loads, fully prestressed concrete members are designed to prevent cracking, which results in reduced section geometry and can lead to durability problems within the concrete. Therefore, allowable limits exist for the tension fibers of prestressed concrete members under service loads.

According to research performed by Liniers[2], the tensile strength of concrete is reduced after concrete is subjected to short-term loading in compression above $0.4f_{ci}'$. These results indicate that further increasing the fiber stresses above the current allowable $0.6f_{ci}'$ may result in cracking of prestressed members at reduced levels. It is unclear whether Liniers[2] work tested normal strength or high strength concrete.

Smadi and Slate[3] performed an X-ray investigation of high-strength concrete (HSC) subjected to sustained stress levels between 40 and 95% of ultimate compressive strength. They found that HSC exhibited significantly less microcracking than normal strength concretes. When cylinders were subjected to sustained loading up to 65% of ultimate strength, HSC had negligible cracking.

If the sustained stress was increased to 80%, cracking increased significantly, leading to nonlinear creep behavior. The majority of cracking below 80% sustained stress consisted of bond cracks between mortar and aggregate.

At a specific section at midspan, the bottom fiber of a prestressed girder is subjected to the highest compressive stress at release, and to the highest tension stress under service loading. To investigate service load performance, Birrcher et al.[4] investigated the effect of increasing the allowable compressive fiber stress on the cracking moment. They found that current design procedures overestimated the cracking load and that overstressing may result in nonlinear material behavior at service loads. They conclude that increasing the limit to a maximum of $0.70f_{ci}'$ may be possible pending full scale testing results.

## RESEARCH PROGRAM

This research program explored the performance of prestressed concrete girders subjected to elevated compressive fiber stresses at release of prestressing. It was divided into two phases: measurement of time-dependant prestress losses and quantification of structural performance. The first phase was discussed in detail in Part I[1]; it will be summarized as necessary in the following sections. The second phase included flexural and shear testing of the girders; it is discussed here in detail.

Six reduced scale prestressed concrete girders were cast with targeted release stresses between 60% and 80% of the initial concrete compressive strength. Time-dependant prestress losses were measured at regular intervals for 196 days, and the girders were then subjected to structural testing to failure. Three of the girders were designed and tested for flexural behavior; the other three were designed and tested for shear behavior.

### Concrete Materials

This investigation used a typical Missouri Department of Transportation (MoDOT) approved HS-SCC mix. The design compressive stresses were 8 ksi (55 MPa) at release of prestressing and 10 ksi (69 MPa) at 28 days. The mix contained a coarse aggregate content below that

normally found in most SCC mixes, resulting in a reduced modulus of elasticity (MOE). Further information about the mix design and constituent materials can be found in Part I[1].

**Girder Designs**

The girders were designed according to the specifications of *AASHTO LRFD Bridge Design Specifications*[5] (hereafter called *AASHTO LRFD*), *ACI 318-08 Building Code Requirements for Structural Concrete*[6] (hereafter called *ACI 318*) and the *PCI Design Handbook, Sixth Edition*[7]. Compressive fiber stress limits were disregarded; all other specifications, including allowable tension limits, were followed. To simplify fabrication, all six prestressed girders were cast simultaneously on the same prestressing bed. This process produced identical prestressing layouts and jacking levels for every member, preventing variations in fabrication. A typical cross-section is shown in **Figure 1**, with cross-sectional properties for all girders shown in **Table 1**. To achieve higher fiber stresses, the entire section width was reduced in ¼ in. (6.4 mm) increments, resulting in a reduced area and moment of inertia. This reduction also resulted in greater strand eccentricity, leading to the higher stresses. As indicated by the test results, the target compressive strength at release of prestressing was not achieved; therefore, compressive fiber stresses were higher than anticipated. Thus the label used for each beam in the following results and discussion corresponds to the actual percentage of concrete fiber stress. Each girder was cast to a length of 15 ft (4.57 m) to ensure full development of prestressing in girders designed for flexural testing.

The flexural reinforcement was designed using strain compatibility with a linear-elastic analysis. As the results indicate, a moment-curvature analysis accounting for non-linear material behavior is a better predictor of structural performance, but the design used linear-elastic strain compatibility. The resulting longitudinal reinforcement consisted of six ½ in. (12.7 mm) diameter, low-relaxation prestressing strands. All strands were straight and fully bonded to the concrete, and all had a manufacturer reported MOE of 28,500 ksi (197,000 MPa) conforming to ASTM A 416[8]. The strands were jacked to 75% of the ultimate strength by the precaster, resulting in an initial stress before any loss of 202.5 ksi (1396 MPa). Elongation measurements taken before and after jacking were used to determine the initial jacking stress.

The detailed method of analysis found in *ACI 318* was used for the shear design due to the improved accuracy of the results. The detailed approach accounts for two types of inclined cracking that can result in a shear failure: flexural-shear and web-shear cracking. Flexural-shear cracking occurs after flexural cracking has taken place, and can lead to shear-compression failure if not properly reinforced. A shear-compression failure occurs when the compression area at the top of the beam, reduced by diagonal tension cracks, is not sufficient to resist the forces resulting from flexure. Web-shear cracking initiates in the web without flexural cracking and can occur in thin webs of highly prestressed beams. For simply supported beams, web-shear cracking typically starts below the neutral axis. This type of inclined cracking is less common than flexural shear cracking. Web-shear cracking occurs when the diagonal (principal) tension stresses reach the tensile strength of the concrete at the center of gravity of the section. Calculations showed that the shear force required to cause flexural-shear cracking was lower than that required to cause web-shear cracking and must, therefore, control the design of shear reinforcement.

Transverse shear reinforcement was designed to accommodate the deficiency in shear capacity, with open-ended U-stirrups (see **Figure 1**) produced from mild steel that conformed to ASTM A 615[9] Grade 60. The girders designed for flexural testing had stirrup spacing, as shown in **Figure 2,** to prevent shear failure. One end of each girder designed for shear testing contained no shear reinforcement, whereas the other end contained stirrups with different spacing, as shown in **Figure 3**. Since this set of girders would be tested in a reduced span, additional closely spaced reinforcement was included at midspan to ensure failure of the ends. The end with no shear reinforcement was designed to test the contribution of concrete and prestressing to the shear performance; the other end tested the additional contribution of shear reinforcement.
When high levels of prestress are applied to members, bursting cracks can develop at the ends due to tensile stresses developed within the prestress anchorage zone. These tensile stresses develop perpendicular to the prestressing compressive forces, and when they exceed the tensile strength of concrete, cracks develop. *AASHTO LRFD* Article 5.10.10.1 addresses anchorage zones in pretensioned concrete members. It requires enough vertical reinforcement in the end zone to provide resistance of at least 4% of the total prestressing force at transfer. The factored bursting resistance of the anchorage zone is calculated from the following equation:

$$P_r = f_s A_s$$

where $f_s$ = the steel stress and is not to exceed a maximum working stress of 20 ksi (137 MPa); and $A_s$ = the area of steel to be placed within a distance of *h/4* from the end of the member. To resist these bursting stresses, an additional stirrup was placed at both ends of each girder, as illustrated in **Figures 2** and **3**.

**Instrumentation**

For Part I[1] on prestress losses, concrete surface strains were measured using a detachable mechanical (DEMEC) strain gauge. These strains were measured from stainless steel DEMEC target points attached to the girders with commercially available metal/concrete epoxy. The DEMEC gauge has an 8 in. (200 mm) gauge length and is calibrated to measure strain to an accuracy of 8.01 x $10^{-6}$ in./in. (mm/mm).

The location of the target points along the section depth is shown in **Figure 4**. Placed at different depths, the points were used to determine the strain profile under applied loads, which was then used to calculate the section curvature and depth to the neutral axis. This calculation provides a check of the theoretical modeling of the member under applied loads. During flexural testing, the loading was stopped at regular intervals so that DEMEC measurements could be taken at each level on the three sets of points along the length of the beam, indicated in **Figure 4.**

The load-deformation relationship was measured using a load cell placed under the hydraulic jack, and linear variable differential transformers (LVDT) located at midspan and at under each of the applied loads. Concrete surface strains at the top fiber were measured using 2 in. (50 mm) long strain gauges, mounted on concrete epoxy.

**Flexure Test Setup**

To develop a constant moment region, the girders were subjected to four-point loading. The supports were located 3 in. (75 mm) from each end of the member. The load was applied with a hydraulic jack located at midspan, and separated into two point loads located 12 in. (458 mm) from midspan by a spreader beam. The flexural test setup is shown in **Figure 5**. The load was applied at an approximate rate of 1000 lb/sec (4.45 kN/sec). Loading was stopped at 10 kips

(44.5 kN), 20 kips (89 kN), 22.5 kips (100 kN) after flexure cracks became visible, and at 30 kips (133.5 kN) to allow for DEMEC measurements and inspection of cracks. Loading was then applied continuously until failure of the girder.

### Shear Test Setup

For each of the three girders tested in shear, two separate tests were performed. The first test was performed to determine the concrete and prestressing contribution to the performance, and the second test examined the shear reinforcement contribution to the performance. This test setup was nearly identical to the flexure setup, but the span length was reduced to 9 ft (2.74 m). Both shear testing setups are shown in **Figure 6**. For all tests, the load was applied at a rate of 1000 lb/sec (4.45 kN/sec) until failure. The loading was not stopped at intermediate points since the location of cracking and failure varied for each girder.

## EXPERIMENTAL RESULTS

### Fresh and Hardened Concrete Properties

The fresh and hardened concrete properties were measured according to applicable standards and guidelines. Fresh properties were found to be typical of SCC used for MoDOT projects. Concrete compressive strength at release (3 days) was 7088 psi (48.8 MPa). The 28 day compressive strength was 9026 psi (62.2 MPa) with an MOE of 4635 ksi (31940 MPa). The concrete strength at 243 days was 8210 psi (56.6 MPa) with an MOE of 4175 ksi (28785 MPa). **Table 2** presents the average, coefficient of variation, and number of concrete cylinder tests at 28, 56, and 243 days. Discussion of the variations in hardened concrete properties can be found in Part I[1].

### Prestress Loss Behavior

As described in Part I[1], the development of prestress losses over time was used to determine the effective prestressing force in the strands. These losses were calculated from three concrete surface strain measurements at midspan, averaged to the center of gravity of the steel. Thus the losses were determined from a total of nine measurements. For the purposes of this discussion,

the total prestress loss measured at test age versus typical prediction methods is presented in **Table 3**[1].

## Predicted Flexural Behavior

For predictions of flexural behavior, several different methods were used to calculate the expected cracking moment (which would be tied to serviceability performance) and the ultimate capacity. The methods used were the *PCI Design Handbook*[7] strain compatibility approach, a layer-by-layer moment curvature analysis similar to that described by Collins and Mitchell[10], and the computer program Response-2000[11]. The moment-curvature and Response-2000 analyses were used to predict the entire load-deformation history; the PCI method was used only to determine cracking loads and ultimate capacity.

Accurate determination of the effective prestressing force is essential to determine the cracking load of prestressed girders. Since the effective prestressing force is tied directly to the amount of prestress loss, accurate determination of those losses affects the accuracy of the predictions. Underestimating of the amount of prestress loss increases the effective prestressing force, resulting in a predicted cracking load that is higher than that of the actual cracking load for the member. In each of these analyses, therefore, the effective prestressing force was determined by two means: first using the predicted prestress losses determined from the Refined Estimates Method of *AASHTO LRFD*, then with the prestressed losses measured in Phase 1 of this research program. The *AASHTO LRFD* Refined Estimates Method was selected because it is commonly used throughout the industry. The effective prestressing force has a lesser impact on the ultimate capacity, because it is determined when the materials fail.

The *PCI Design Handbook*[7] predicts the cracking moment using:

$$M_{cr} = P_{eff} e_{ps} + \frac{P_{eff} S_b}{A_c} + f_r S_b$$

where $M_{cr}$ = the cracking moment, $P_{eff}$ = the effective prestressing force after losses, $e_{ps}$ = the strand eccentricity, $S_b$ = the gross bottom section modulus, $A_c$ = the gross section area, and $f_r$ = the modulus of rupture of concrete, which was assumed to equal 7.5 times the square root of the compressive strength of concrete as defined in the handbook. Like the MOE, the modulus of

rupture is sensitive to the constituent materials. This value was developed from data on conventional and high-strength concrete, but without additional data on SCC it is assumed to be valid. The cracking moment was then converted to cracking load using**:**

$$P = \frac{2\left(M - M_d\right)}{a}$$

where $P$ = the applied load, $M$ = applied moment, $M_d$ = the dead load moment, and $a$ = the distance between the support and the concentrated load.

The ultimate capacity was calculated using the strain compatibility method because the handbook notes that this method is typically more accurate than standard code equations. The effective strain of the top fiber at failure was assumed to be 0.003 in./in. (mm/mm). This correlates well with the average strain value of 0.00309 in./in. (mm/mm), measured using two strain gauges mounted on top of each girder during loading and taken from **Table 4**. The effective prestress was determined for each individual layer, and standard principles of mechanics were used to determine the ultimate moment capacity. Using these values, the ultimate load was determined from the equation above.

Moment-curvature analysis was chosen to predict behavior since it has been widely used to analyze structures. Moment-curvature analysis provides a more detailed and accurate prediction of the deflection and flexural capacity of a member and explains the behavior of the member in progressive load stages leading to failure. This method develops a rational analysis that follows the behavior of the bonded prestressed concrete beam through the total load range from initial loading to failure stage. To improve the results, the analysis was performed using the layer-by-layer method, dividing the cross-section into several layers. The top fiber strain in the concrete and the position of the neutral axis are assumed to obtain the concrete strain distribution. The stress-strain profile used for concrete was the relationship developed by Thorenfeldt et al.[10], while the Modified Ramberg-Osgood[10] function was used for the prestressing. Prior to concrete cracking, the moment-curvature analysis produces results similar to the behavior predicted by the *PCI Design Handbook* method since the girders are assumed to remain linear elastic. Post-cracking response was determined using the layer-by-layer method, and the resultant concrete stress was found using:

$$C_c = \sum A_{ci} f_{ci}$$

where $A_{ci}$ = the area of each individual concrete layer and $f_{ci}$ = the stress at the centroid of that layer, determined from the calculated strain and Thorenfeldt's equation. The resultant steel stress was found using:

$$T_s = \sum A_{ps} f_{pe}$$

where $A_{ps}$ = the area of each layer of tendons and $f_{pe}$ = the effective prestress after losses. Therefore, for a given top fiber strain the depth to the neutral axis can be found when the resultant concrete and steel stresses are equal. The moment is found by multiplying each resultant force with the distance to the neutral axis and adding the results. The corresponding curvature will equal the strain in the top fiber divided by the depth to the neutral axis. Increasing the assumed top fiber strain results in increased force resultants and moments, which are used to develop the moment curvature response. The calculated moments were translated into load using the earlier equation. The conjugate beam method was used with numerical integration to calculate the girder deflections from the curvature along the member:

$$\Delta = \left( \frac{\phi_1 x_1 + \phi_2 x_2}{2} \right) \Delta x_1 + \left( \frac{\phi_2 x_2 + \phi_3 x_3}{2} \right) \Delta x_2 + .....$$

where $\Delta$ = the midspan displacement, $\phi$ = the curvature at a specific point $x$, and $\Delta x$ = the distance between two points.

The computer program Response-2000[11] performs calculations similar to those involved in moment-curvature analysis. The analyses produced slightly different predictions of elastic behavior, and the computer program included the effect of tension stiffening in the post-cracking response.

**Flexure Results**

In reinforced or prestressed concrete, flexural cracks form when the tensile stress of the bottom fiber of the member exceeds the modulus of rupture of the concrete. Prior to this point, the member behaves in a linear-elastic fashion according to Hooke's Law. Therefore, the cracking load can be determined from the load-deformation plot when that relationship no longer appears linear. **Figures 7**, **8**, and **9** demonstrate the method used to determine the approximate cracking load for girders B-84, B-75, and B-68. As an alternative to estimating from the plots, the

cracking load can also be approximated from the strain measured using the DEMEC points mounted on the sides of the girders. Since loading was stopped at 10 and 20 kips (44.5 and 89 kN), and given that the strain was assumed to have a linear distribution, the strain at the bottom fiber can be extrapolated from the measurements. Using those data points, the cracking load could be estimated by interpolating between 10 and 20 kips (44.5 and 89 kN) until the bottom fiber strain equaled the strain at the modulus of rupture. As a result, the values estimated from the plots and those determined from the strain profile were relatively in agreement. The estimated cracking loads for the three girders are shown in **Table 5**.

**Table 5** compares cracking loads predicted by the three methods described above with actual cracking loads. The effective prestressing force has a significant impact on the predicted cracking load, so the predictions were calculated using both predicted prestress losses and measured prestress losses. **Figure 10** presents the data shown in **Table 5** as a ratio of the measured to the predicted cracking load. It shows that all three methods, using both predicted and measured losses, underestimated the cracking load by less than 16%. Such underestimation results in a conservative prediction of member behavior. Birrcher et al.[4] performed a similar analysis on HSC girders subjected to elevated compressive fiber stresses at release. They found the procedure outlined in the *PCI Design Handbook* and *AASHTO LRFD 2005 Interim Specifications*[12] for prediction of prestress losses and cracking loads overestimated the actual cracking load. The *PCI Design Handbook* method overestimated the cracking load by an average of 10.2%, with a high of 22.5%, and the *AASHTO LRFD 2005 Interim Specifications* overestimated by an average of 4.4%, with a high of 13%. Since they calculated cracking load based only on estimated prestress losses, the accuracy of the predicted capacity was dependant on the accuracy of those estimations.

The complete load-deflection relationship for girders B-84, B-75, and B-68 is shown in **Figures 11, 12,** and **13**, respectively. These figures also show the predicted response according to the moment-curvature analysis and Response-2000[11]. They demonstrate that the author developed moment-curvature analysis is a better predictor of linear-elastic behavior, whereas Response-2000[11] better predicts inelastic behavior, because the software considers tension stiffening in its calculations. **Table 6** compares predicted and measured ultimate moment capacity, and **Figure**

**14** plots the ratio of measured to predicted ultimate capacity for all three girders. The latter figure indicates that each method predicts the ultimate capacity to within 14%, with the more advanced analysis improving accuracy. Similar to the cracking load, ultimate capacity is also underestimated by all three prediction methods, leading to conservative predictions. The difference between ultimate capacity calculated from predicted losses and from measured losses demonstrates that variations in the effective prestressing force have a relatively small impact on predictions of ultimate capacity.

The displacement of members subjected to bending is dependant on the stiffness of the member, and specifically on the inverse of the stiffness. The member stiffness is determined from the MOE of the material and the moment of inertia. Since all girders were cast simultaneously, the MOE is assumed to be uniform among them, thus the only difference is the geometrical properties of the members. Therefore, normalization can permit comparison of the load-displacement relationship for members of various sizes. **Figure 15** presents the load-displacement relationship for all three girders normalized to the stiffness of B-64. It indicates that the relative flexural behavior of each girder is very similar except for ultimate capacity of the member, which is tied to the width of the compression block.

**Predicted Shear Behavior**

The behavior of members subjected to shear is not as well understood as those subjected to flexure. The predicted behavior of flexural members follows conventional principles of material properties and strain compatibility, whereas shear capacity has traditionally been predicted using empirical relationships.

Both *AASHTO LRFD* and *ACI 318-05* use empirical equations to determine the contribution of concrete, whether prestressed or non-prestressed, to the total shear capacity of the member. Since the shear capacity of concrete is closely related to the mix proportions, and especially to the coarse aggregate content, empirical equations developed for normal strength concrete may not apply to high-strength or self-consolidating concrete. This project determined the shear capacity using the detailed method outlined in *ACI 318* and discussed in the *PCI Design Handbook*. For the girder ends without shear reinforcement, the expected capacity was

calculated from the limiting value of web-shear and flexure-shear cracking. For all three girders, flexure-shear was found to be deficient in an area approximately 12 in. (30.5 cm) wide next to the applied concentrated load. For the girder ends with shear stirrups, the smaller shear capacity was smaller in the same area next to the support, but it had a larger value due to the contribution from shear reinforcement. The contribution from the shear reinforcement was determined according to *ACI 318* Section 11.5.7.2 which assumes that cracks are inclined at 45°.

The computer program Response-2000[11] predicts shear capacity based on the Modified Compression Field Theory and was used to analyze the girders with and without shear reinforcement. The program calculates the capacity at various sections along the girder length and determines the minimum load causing failure.

**Shear Results**

The typical method used to visualize shear behavior is the plot of shear force (or stress) versus shear strain. The shear force was easily determined from load tests, since it is equal to the applied force. The shear strain, however, was not as easily measured since the location of shear failure (i.e., the point where the shear strain was greatest) occurred at varying points along the girders. For simplicity and to maintain uniformity with the flexural tests, therefore, the shear behavior was plotted as the relationship between load (shear) and displacement at the point of load.

Bursting cracks developed at the ends of the member, reducing the shear capacity of some members. As noted above, the design of prestressed members must be checked to control high tensile forces that develop perpendicular to the prestressing strands and often lead to cracking. For this set of girders, cracking did not occur instantaneously with the release of prestressing, rather, cracks developed as concrete shrinkage and creep added additional stresses. On seven of the 12 member ends, these cracks occurred at one level of prestressing and extended in from the end between 6 and 18 in. (15 and 46 mm). The cause of these cracks was most likely the increased level of prestressing applied to achieve the high fiber stresses demanded by the research program. These bursting cracks did not influence the flexural behavior, but they did appear to contribute to in the reduction of shear capacity.

The load displacement relationships, both with and without shear reinforcement, are shown in **Figures 16**, **17**, and **18** for girders B-79, B-72, and B-68, respectively. In each of these figures, the point where the relationship is no longer linear signifies development of shear cracks within the girders, and the transfer of shear to the transverse reinforcement. This point corresponds to a value slightly larger than the shear capacity of the concrete because some of the shear force is already transferred to the transverse reinforcement. **Figure 19** compares the load-displacement relationship for the ends of the girders without shear reinforcement, and **Figure 20** compares the relationship for the ends of the girders with shear reinforcement. Both of these figures indicate little difference in behavior aside from the differing amounts of shear reinforcement.

**Figures 21** through **26** show the crack patterns of each of the failed tests. The bursting cracks are visible and their influence on the failure of the girders is apparent. When the bursting cracks extended well into the beam, the shearing forces widen them, and failure extended from them. In members without shear reinforcement, cracks developed beside the support and extended directly to the applied load, similar to deep beam behavior with a direct compression strut. The cracking was typically initiated in the web, indicating web-shear failure, which does not match the design calculations. Due to the small inclination (less than 16°) of the compression strut and the reinforcement configuration, a strut-and-tie model produced unreliable results. In members with shear reinforcement, flexure cracks developed first, followed by shear cracking through a stirrup, indicating flexure-shear failure as predicted. The crack inclination on these members was approximately 45°, as assumed in the design equation.

**Table 7** compares measured shear capacity with the predicted shear capacity outlined above for the ends without shear reinforcement. **Table 8** presents a similar comparison for the ends with reinforcement. Both of these tables indicate that shear failure occurred below the predicted shear capacity in nearly every test. The only underestimation of capacity occurred using the PCI Method on B-65, with an error of 11.6%. For the remaining predictions, the error ranged between 2.4% and 99% overestimation. Test results reported by Naito et al.[13] showed similar behavior in girders produced with SCC and those produced with HESC, with actual capacity exceeding predicted capacity. The results reported here and the failure patterns shown in

**Figures 21** through **26** indicate that, to ensure adequate safety, additional testing is recommended for girders produced using normal and higher strength SCC with lower coarse aggregate contents.

## CONCLUSIONS

Numerous factors affect the structural performance of prestressed concrete members, especially concrete properties. The conclusions drawn here, therefore, are applicable to members produced at the sponsoring production plant in Missouri. The results of the experimental program described here, along with the results from Phase I of this program on prestress losses, suggest the following conclusions:

1. Self-consolidating concrete produced with lower coarse aggregate contents reduces the MOE of the concrete. Further investigation is needed of the effect of reduced modulus values on the overall performance of prestressed concrete.
2. The methods presented here for predicting the cracking load are conservative compared to experimental results. All these methods underestimated the cracking load to within 16% of the measured value.
3. These methods also provide conservative predictions of the ultimate capacity of the section. All underestimated capacity to within 14% of the actual capacity.
4. Following the change of allowable compressive stress at the ends included in *ACI 318*, an increase in the allowable stress limit to at least $0.70f`_c$ at any point along the member is recommended. Increasing the allowable compressive fiber stress at release of prestressing to 75% at any point along the member appears feasible when the member is designed for flexure. Typical prestressed girders in service have uniformly distributed dead loads and do not perform in the same way as the tested specimens which performed similar to deep beams; therefore the shear performance is less critical.
5. The shear capacity of girders produced using reduced coarse aggregate content SCC is uncertain. Based on the limited results presented here, their capacity is well below the capacity predicted using current design equations. Further testing is needed to ascertain the impact of low coarse aggregate content on the shear performance of SCC girders.
6. End region cracking is of concern due to its impact on shear performance. End region cracking should be studied in full-scale SCC girders to evaluate the need for further

research, particularly if the use of SCC mixes with reduced aggregate contents is continued to maintain SCC flowability.

## ACKNOWLEDGEMENTS

The authors would like to acknowledge the financial support of Coreslab Structures, Inc. in Marshall, Missouri and that of the Center for Transportation Infrastructure and Safety (CTIS) at the Missouri University of Science and Technology (formerly the University of Missouri-Rolla). We also thank the engineers and personnel at Coreslab Structures, Inc. for their contributions during planning and production. And we are grateful for the technician and staff support from the Center for Infrastructure Engineering Studies (CIES) and Department of Civil, Architectural, and Environmental Engineering at the Missouri University of Science and Technology for their support of this work.

## REFERENCES


1. Brewe, J. and Myers, J. J.; "High-Strength Self-Consolidating Concrete Girders Subjected to Elevated Compressive Fiber Stresses, Part I: Prestress Loss and Camber Behavior," *PCI Journal*, In preparation
2. Liniers, A.D.; "Microcracking of Concrete under Compression and Its Influence on Tensile Strength," *Materials and Structures*, V. 20, No. 116, March 1987, pp. 111-116
3. Smadi, M.M.; Slate, F.O.; "Microcracking of High and Normal Strength Concretes under Short- and Long-Term Loadings," *ACI Materials Journal*, V. 86, No. 2, March-April 1989, pp. 117-127
4. Birrcher, D.B.; Tuchscherer, R.G.; Mraz, D.; Castro, A.; Bayrak, O.; and Kreger, M.E.; "Effects of Increasing the Allowable Compressive Release Stress of Pretensioned Girders," *2006 Concrete Bridge Conference*, Grapevine, TX, 20 pp
5. American Association of State Highway and Transportation Officials, *AASHTO-LRFD Bridge Design Specifications*, Fourth Edition, Washington, DC (2007)
6. American Concrete Institute (ACI 318-05), *Building Code Requirements for Structural Concrete*, American Concrete Institute, Farmington Hills, MI (2005)
7. Precast/Prestressed Concrete Institute, *PCI Design Handbook, Precast and Prestressed Concrete*, Sixth Edition, Chicago, IL (2004)
8. ASTM A 416, Standard Specification for Steel Strand, Uncoated Seven-Wire for Prestressed Concrete, ASTM International, West Conshohocken, PA
9. ASTM A 615, Standard Specification for Deformed and Plain Carbon-Steel Bars for Concrete Reinforcement, ASTM International, West Conshohocken, PA
10. Collins, M.P. and Mitchell, D.; *Prestressed Concrete Structures*, Prentice-Hall, Inc., 1991
11. Bentz, E.; *Response-2000 Version 1.1*, Department of Civil Engineering, University of Toronto, 2001
12. American Association of State Highway and Transportation Officials, *AASHTO-LRFD Bridge Design Specifications*, Third Edition, Washington, DC, Interim 2005
13. Naito, C.J.; Parent, G.; and Brunn, G.; "Performance of Bulb-Tee Girders Made with Self-Consolidating Concrete," *PCI Journal*, V. 51, No. 6, November–December 2006, pp. 72-85

## NOTATION

$a$ = distance between support and concentrated load

$A_c$ = gross area of section

$A_{ci}$ = area of each individual concrete layer

$A_{ps}$ = area of each layer of prestressing tendons

$A_s$ = area of mild steel

$e_{ps}$ = prestressing strand eccentricity

$E_{ps}$ = modulus of elasticity of prestressing strands

$E_{ci}$ = modulus of elasticity of concrete at release

$f_{ci}$ = stress at the centroid of concrete layer

$f_{pe}$ = effective prestress after losses

$f_r$ = modulus of rupture of concrete

$M$ = applied moment

$M_{cr}$ = cracking moment

$M_d$ = dead load moment

$P$ = applied load

$P_{eff}$ = effective prestressing force after losses

$S_b$ = gross bottom section modulus

$\Delta$ = midspan displacement

$\phi$ = curvature at a specific point

$\Delta x$ = distance between two points

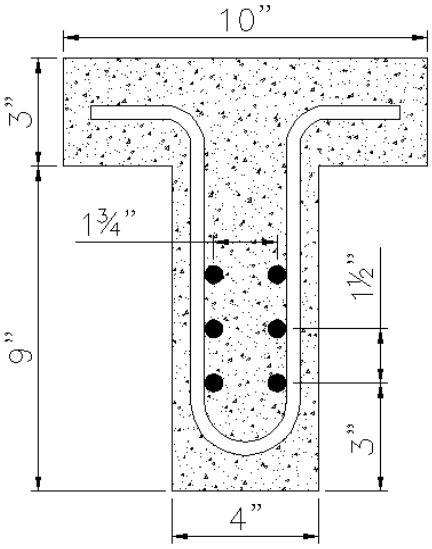


**Figure 1** – Typical Cross-Section

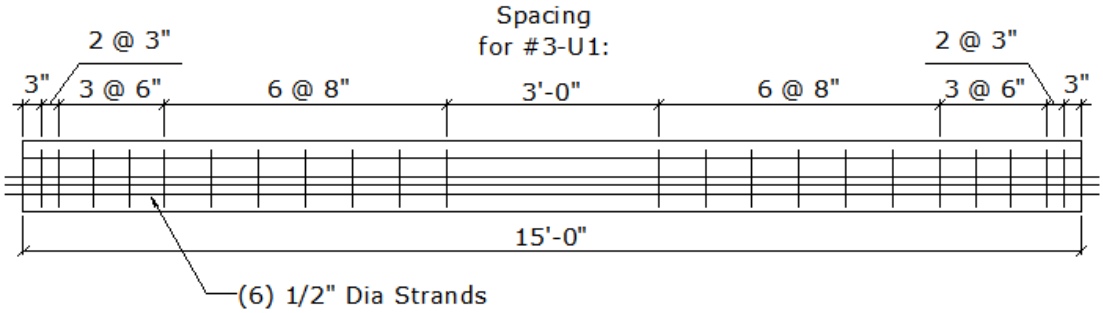


**Figure 2** – Shear Stirrup Spacing for Flexural Girders

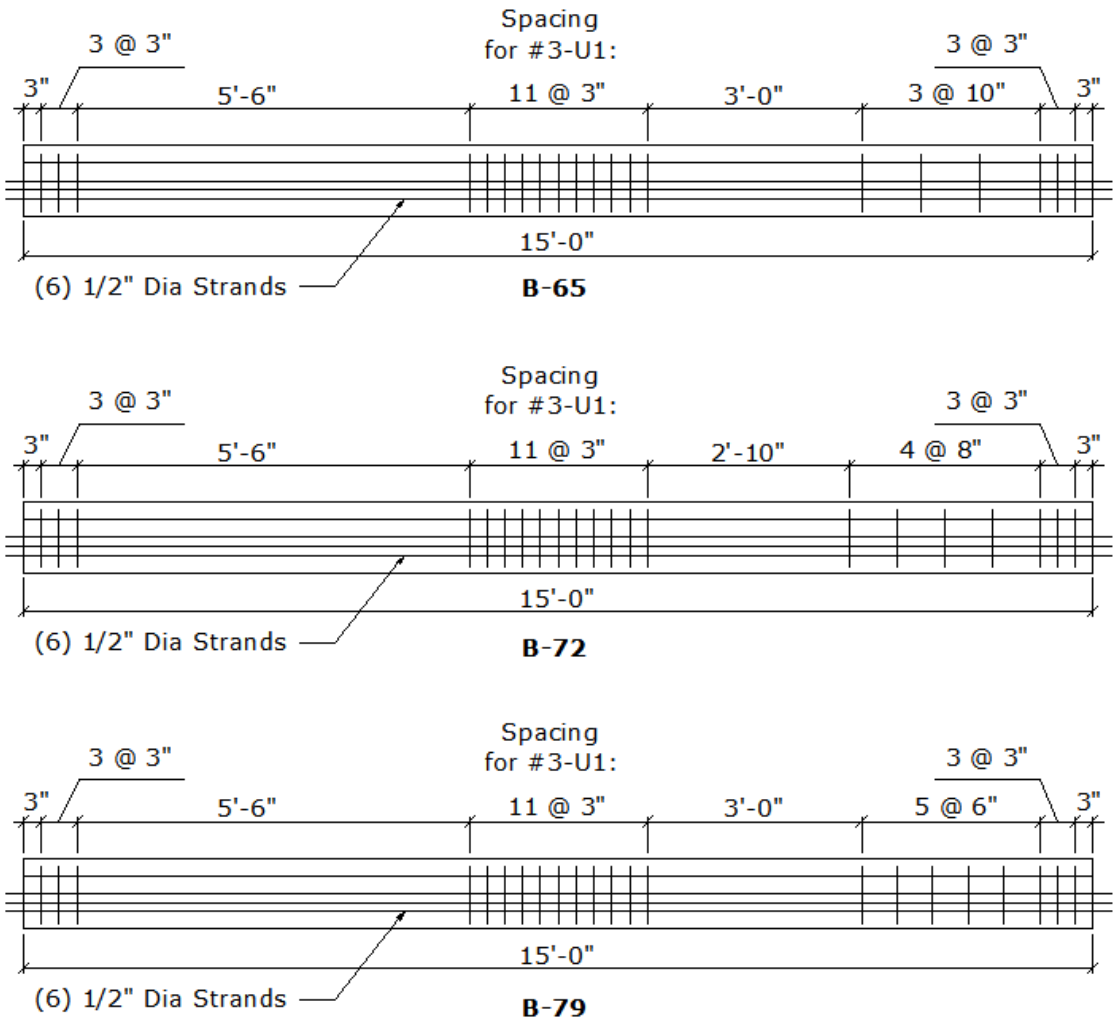


**Figure 3** – Shear Stirrup Spacing for Shear Girder Tests

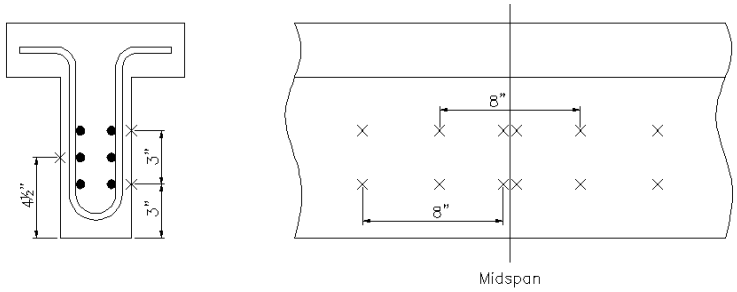


**Figure 4** – Location of DEMEC Target Points

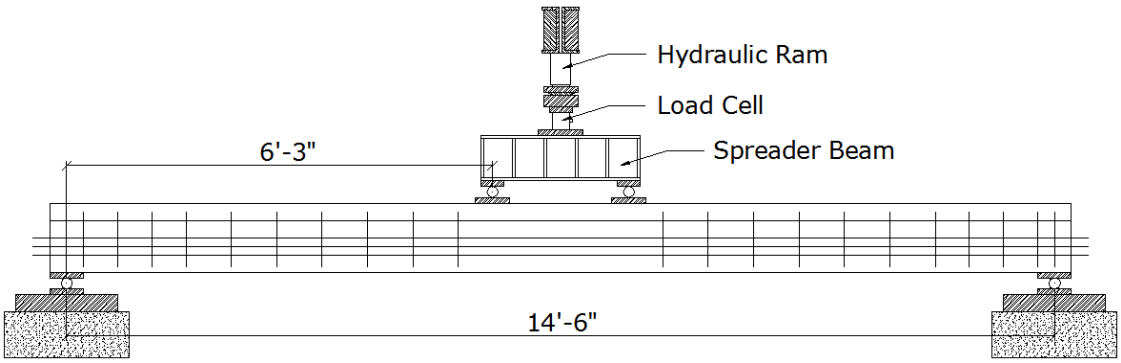


**Figure 5** – Flexure Test Setup

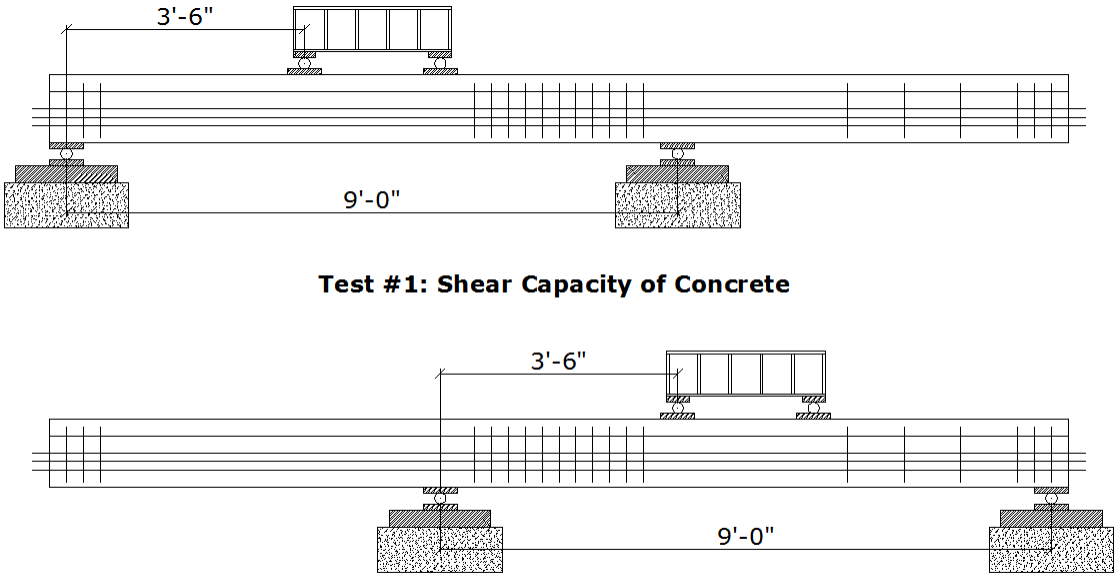


**Figure 6** – Shear Test Setup

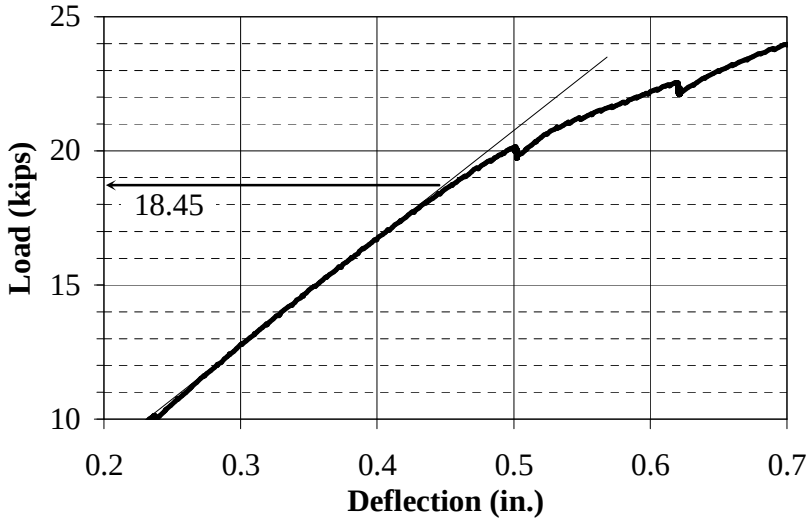


**Figure 7** – Estimation of Cracking Load from B-84 Load-Displacement Plot
Note: 1 kip = 4.45 kN, 1 in. = 25.4 mm

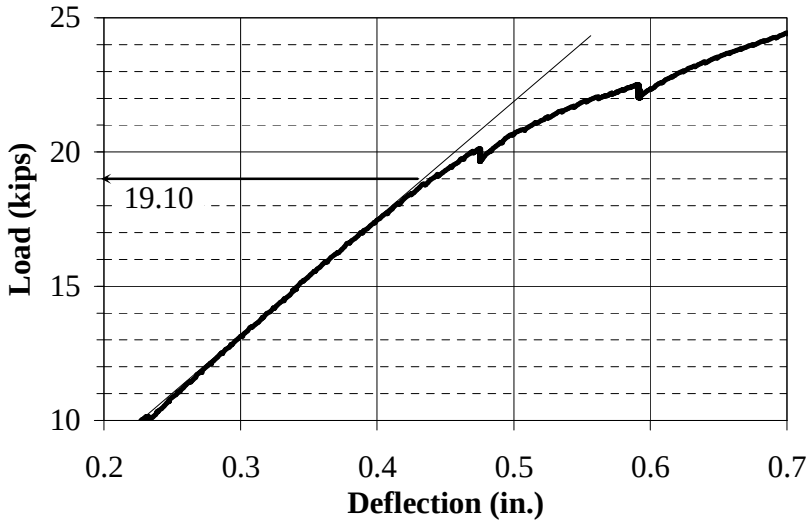


**Figure 8** – Estimate of Cracking Load from B-75 Load-Displacement Plot
Note: 1 kip = 4.45 kN, 1 in. = 25.4 mm

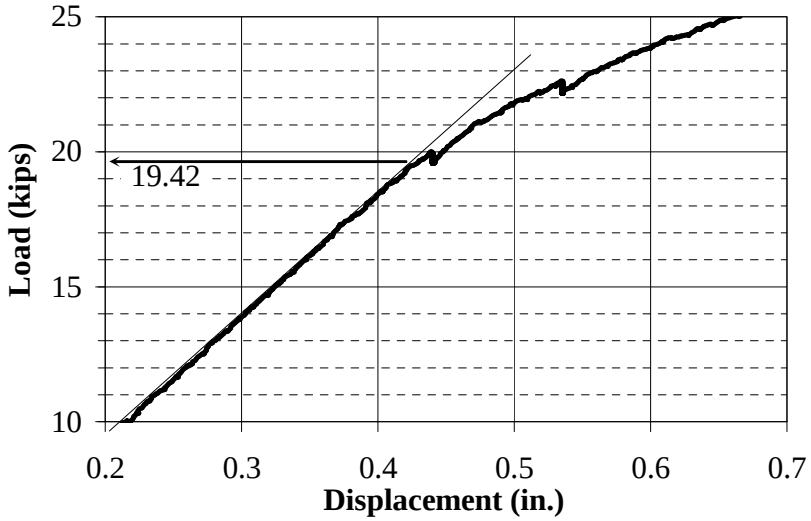


**Figure 9** – Estimation of Cracking Load from B-68 Load-Displacement Plot
Note: 1 kip = 4.45 kN, 1 in. = 25.4 mm

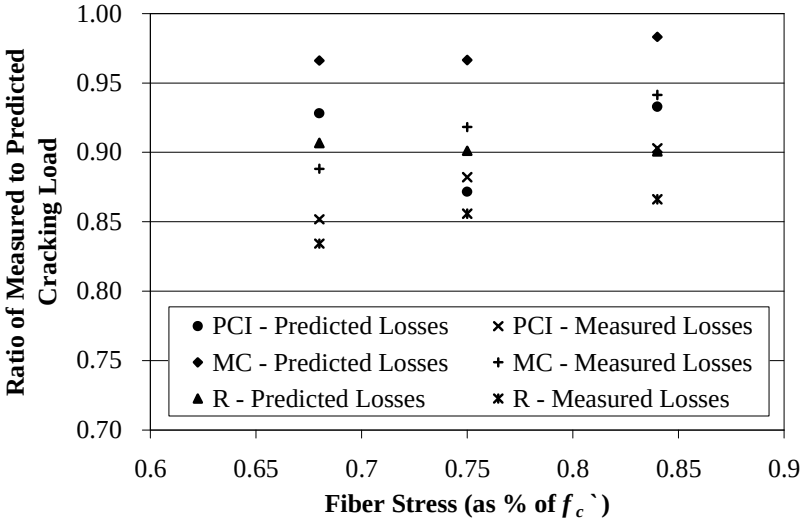


**Figure 10** – Comparison of Predicted versus Calculated Cracking Load

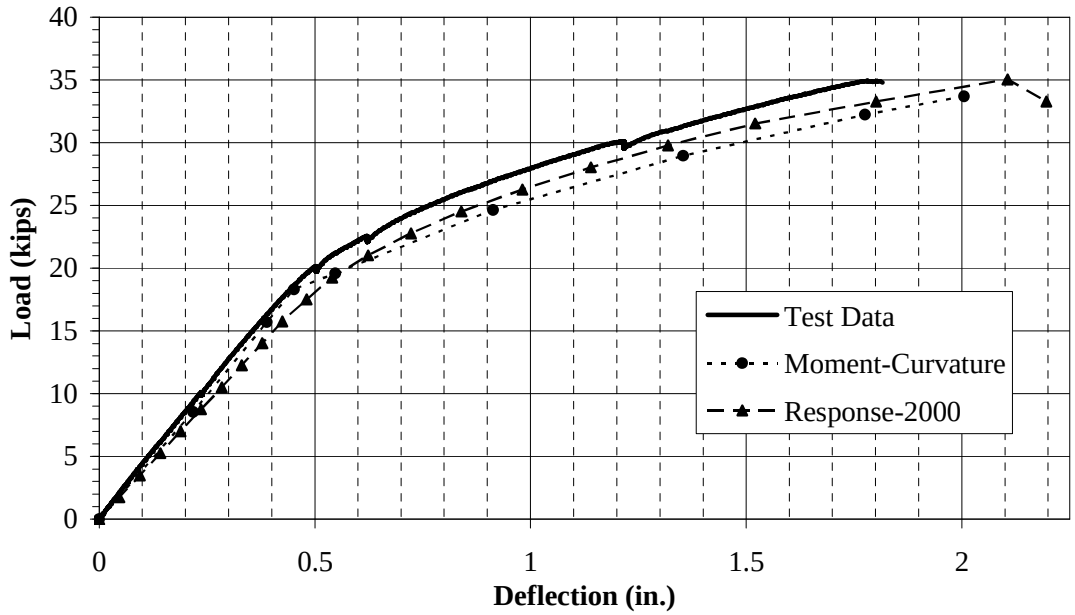


**Figure 11** – Load-Displacement Relationship for B-84
Note: 1 kip = 4.45 kN, 1 in. = 25.4 mm

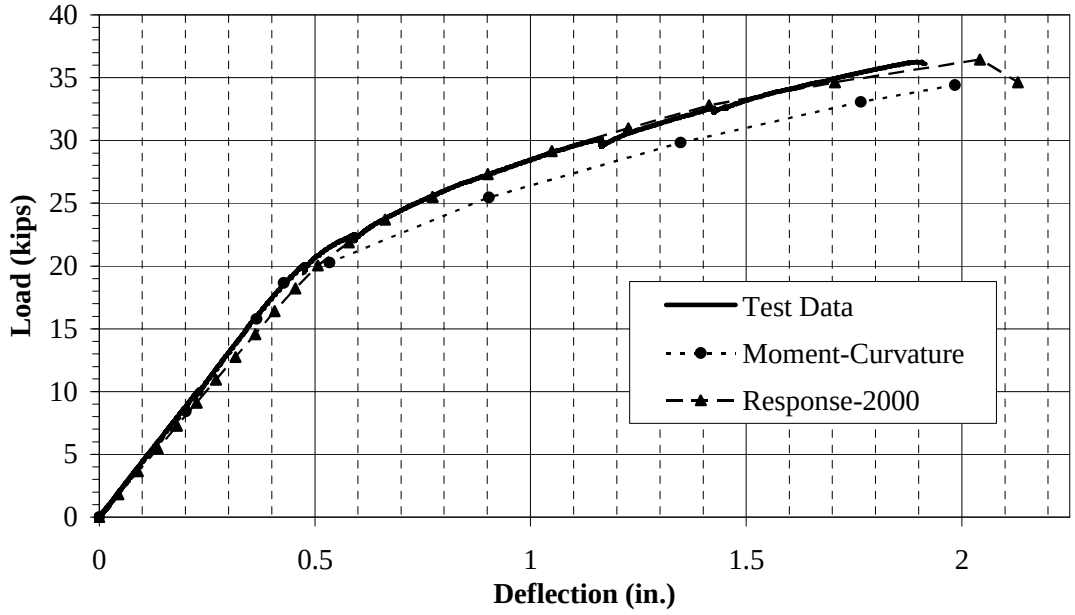


**Figure 12** – Load-Displacement Relationship for B-75
Note: 1 kip = 4.45 kN, 1 in. = 25.4 mm

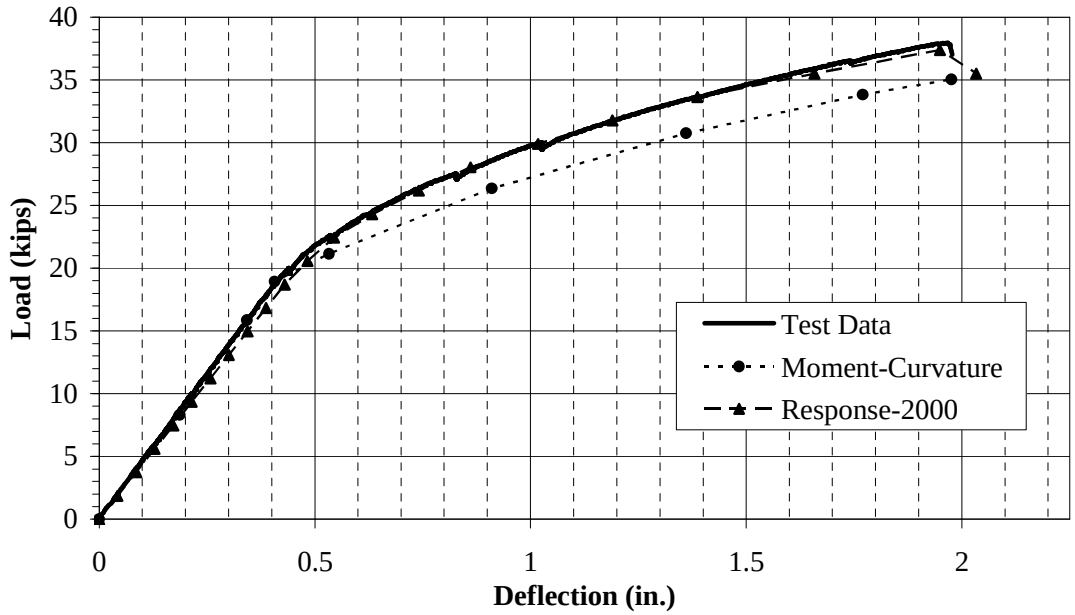


**Figure 13** – Load-Displacement Relationship for B-68
Note: 1 kip = 4.45 kN, 1 in. = 25.4 mm

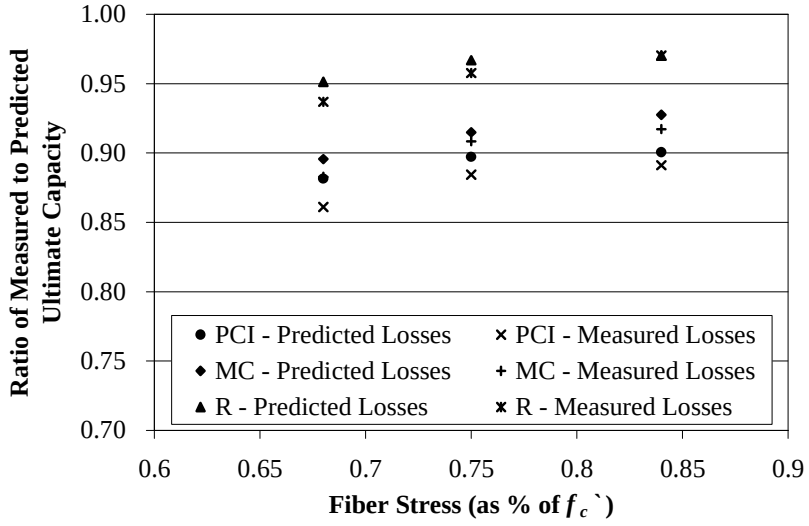


**Figure 14** – Comparison of Predicted versus Calculated Ultimate Capacity

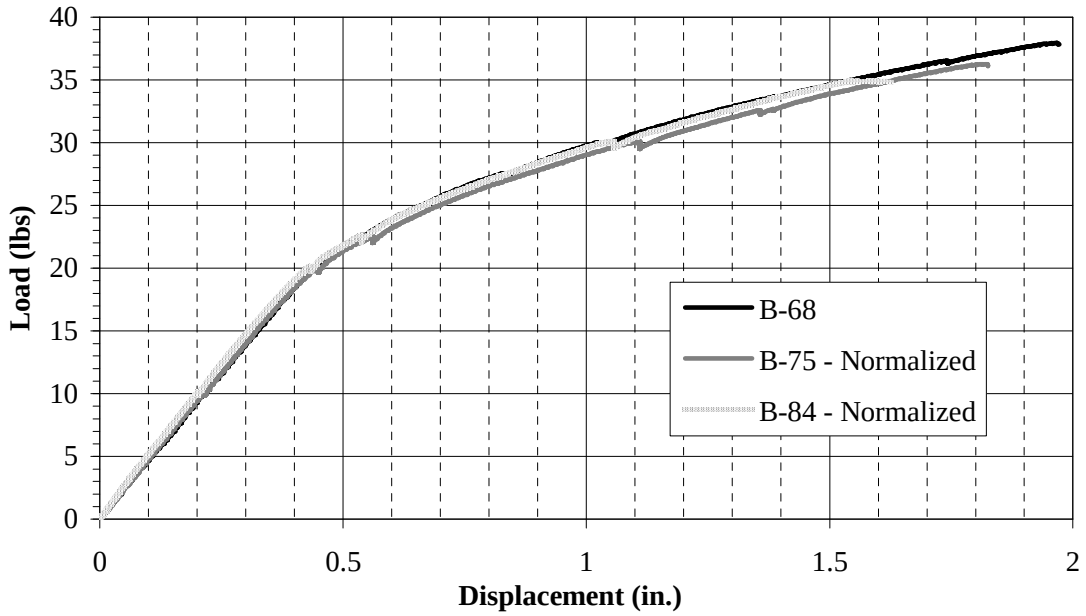


**Figure 15** – Load-Displacement Relationship Normalized to B-68
Note: 1 kip = 4.45 kN, 1 in. = 25.4 mm

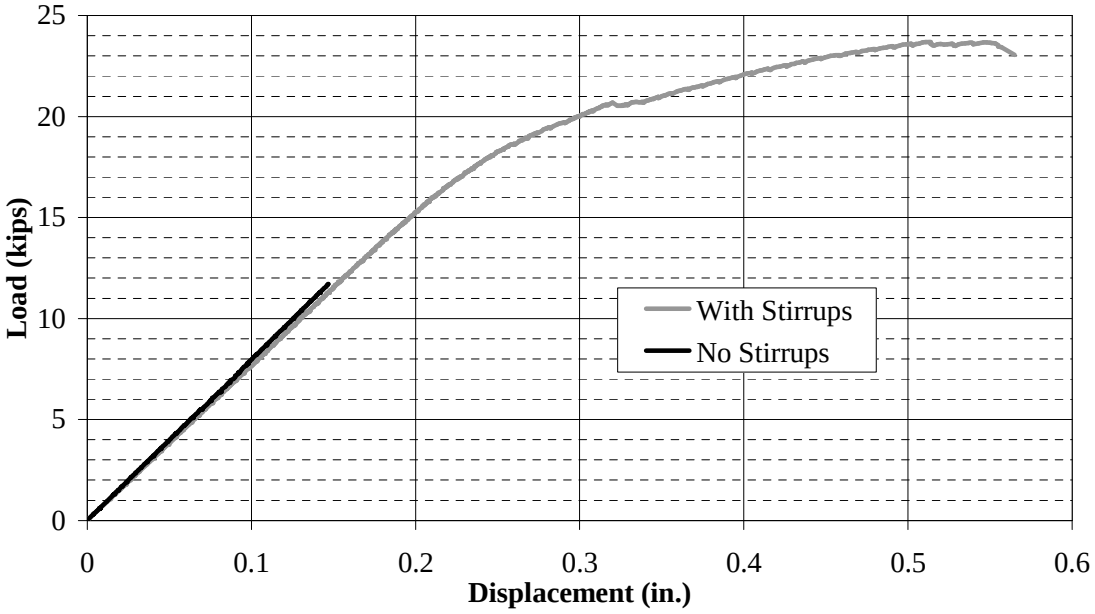


**Figure 16** – Shear Behavior of B-79
Note: 1 kip = 4.45 kN, 1 in. = 25.4 mm

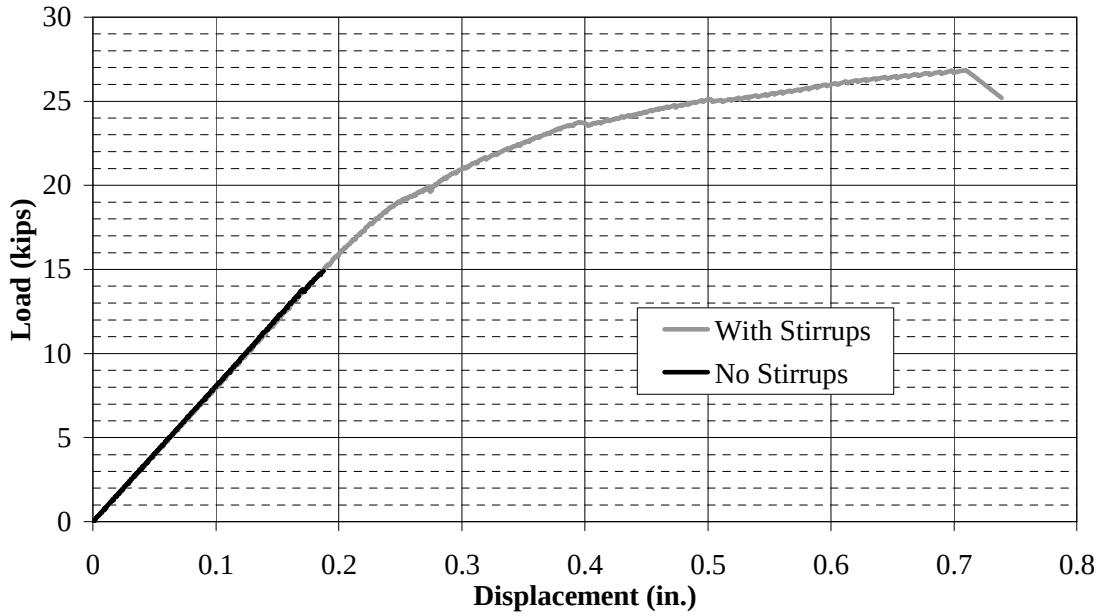


**Figure 17** – Shear Behavior of B-72
Note: 1 kip = 4.45 kN, 1 in. = 25.4 mm

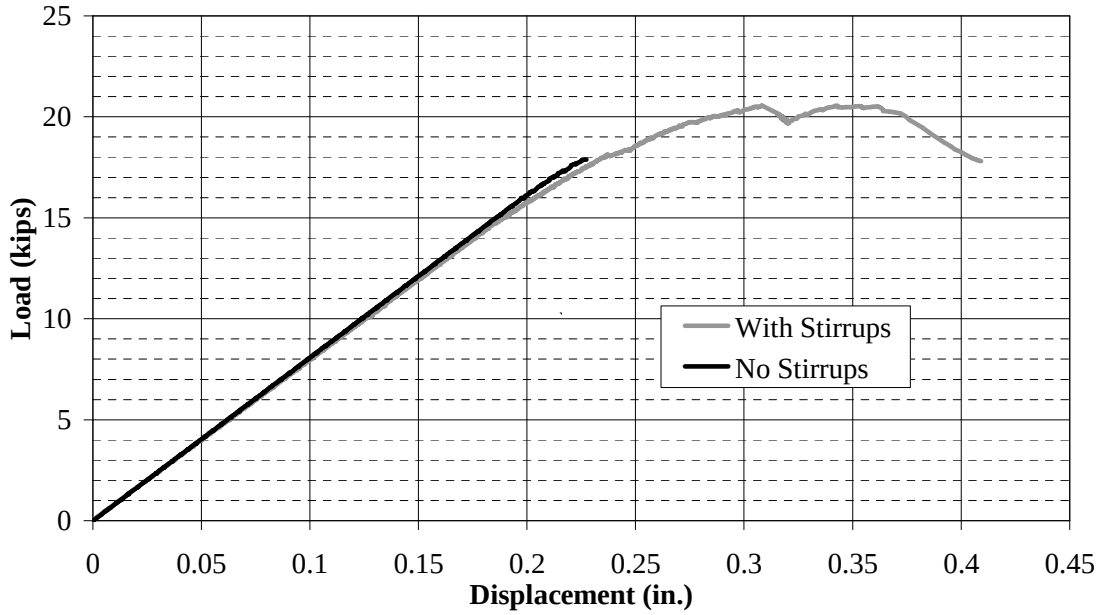


**Figure 18** – Shear Behavior of B-65
Note: 1 kip = 4.45 kN, 1 in. = 25.4 mm

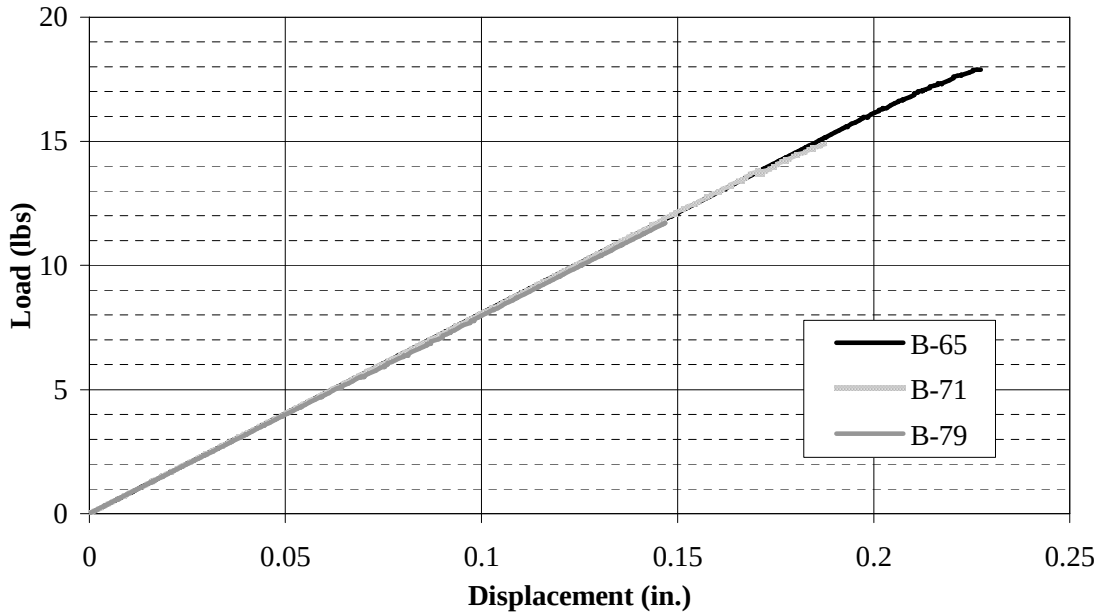


**Figure 19** - Comparison of Shear Behavior without Stirrups
Note: 1 kip = 4.45 kN, 1 in. = 25.4 mm

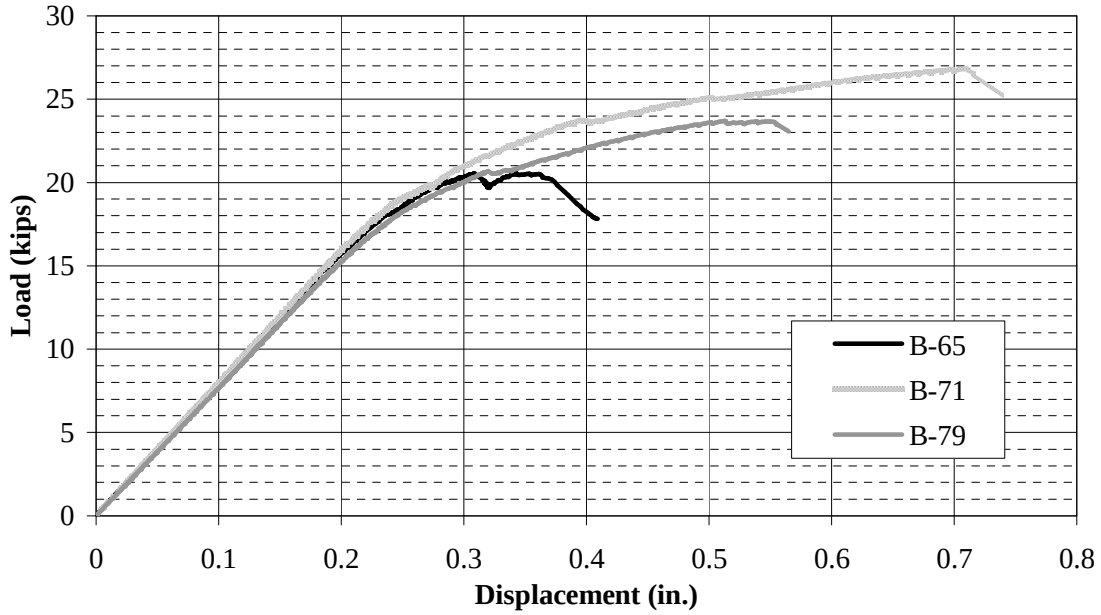


**Figure 20** – Comparison of Shear Behavior with Stirrups
Note: 1 kip = 4.45 kN, 1 in. = 25.4 mm

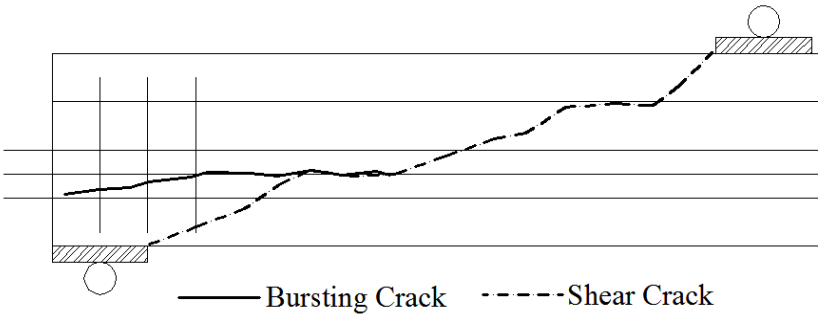


**Figure 21** – Shear Failure of B-65 with No Stirrups

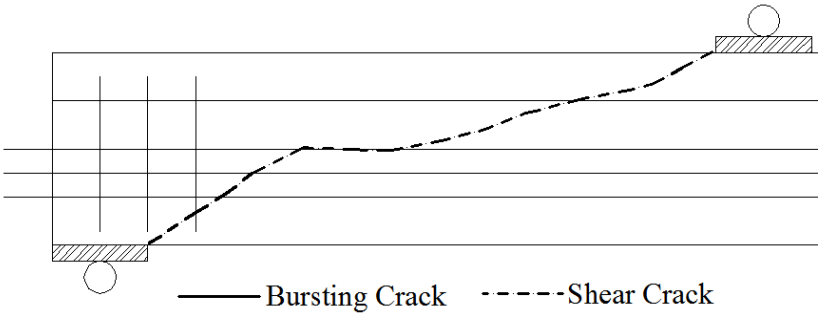


**Figure 22** – Shear Failure of B-72 with No Stirrups

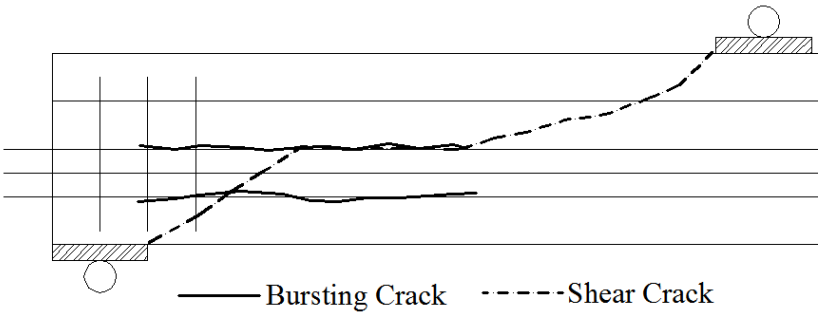


**Figure 23** – Shear Failure of B-79 with No Stirrups

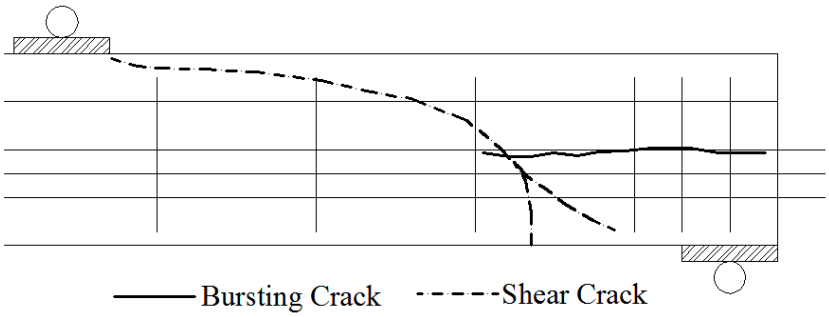


**Figure 24** – Shear Failure of B-65 with Stirrups

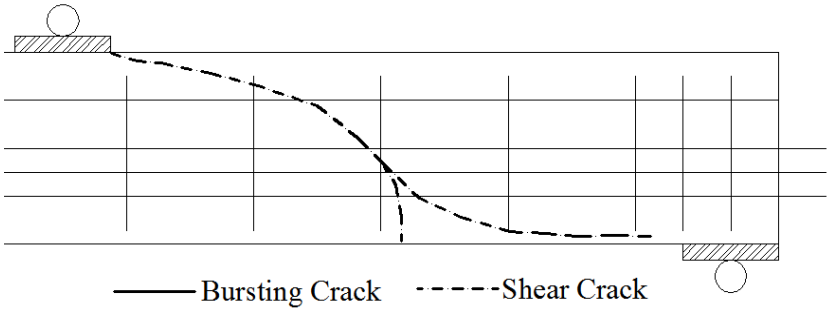


**Figure 25** – Shear Failure of B-72 with Stirrups

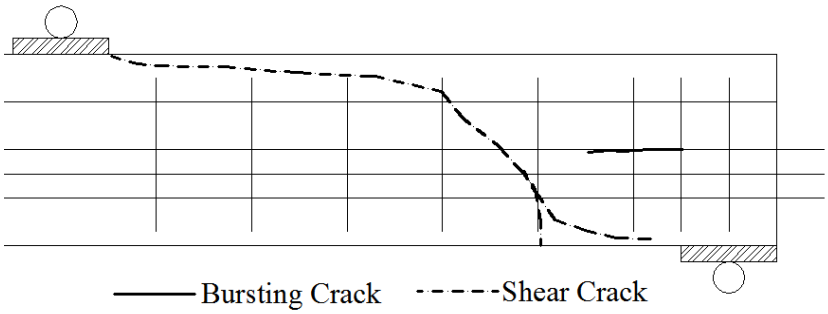


**Figure 26** – Shear Failure of B-79 with Stirrups

**Table 1** - Beam Cross-Sectional Properties

| Girder Designation | B-84 | B-79 | B-75 | B-71 | B-68 | B-65 |
|---|---|---|---|---|---|---|
| Target Stress Level (% of $f`_{ci}$) | 80 | 75 | 71 | 68 | 64 | 60 |
| Actual Stress Level (% of $f`_{ci}$) | 84 | 79 | 75 | 71 | 68 | 65 |
| Gross Area, $A_g$ ($in^2$) | 66 | 69 | 72 | 75 | 78 | 81 |
| Gross Moment of Inertia, $I_g$ ($in^4$) | 855 | 895 | 935 | 975 | 1014 | 1053 |
| Distance from CGC to Top Fiber, $y_t$ (in) | 4.77 | 4.83 | 4.88 | 4.92 | 4.96 | 5.00 |
| Distance from CGC to Bottom Fiber, $y_b$ (in) | 7.23 | 7.17 | 7.13 | 7.08 | 7.04 | 7.00 |
| Strand Eccentricity, $e_p$ (in) | 2.73 | 2.67 | 2.63 | 2.58 | 2.54 | 2.50 |
| Distance from Top Fiber to CGS, $d_p$ (in) | 7.50 | | | | | |

Note: CGC = center of gravity of concrete, CGS = center of gravity of steel; 1 in.= 25.4 mm

**Table 2** – Hardened Concrete Properties

| Test Age | 28 days | 56 days | 243 days |
|---|---|---|---|
| Average Compressive Strength (psi) | 9026 | 9024 | 8210 |
| Coefficient of Variation | 0.80% | 1.41% | 1.94% |
| Number of Compression Tests | 3 | 3 | 6 |
| Average MOE (ksi) | 4635 | – | 4175 |
| Predicted MOE[1] (ksi) | 5082 | – | 4847 |
| Ratio of Measured to Predicted MOE | 0.912 | – | 0.861 |

Note: 1 ksi = 6.89 MPa, 1 – According to *AASHTO LRFD 5.4.2.4*

**Table 3** – Measured versus Predicted Prestress Losses

| Total Losses at 243 days (ksi) | | | | | | |
|---|---|---|---|---|---|---|
| **Designation** | **B-84** | **B-79** | **B-75** | **B-71** | **B-68** | **B-65** |
| Measured | 66.5 | 70.7 | 64.5 | 62.9 | 67.4 | 57.7 |
| *AASHTO LRFD 4th Ed.* | 58.7 | 56.3 | 54.2 | 52.2 | 50.3 | 48.6 |
| | -12% | -20% | -16% | -17% | -25% | -16% |
| *PCI* | 88.8 | 84.0 | 79.7 | 75.9 | 72.4 | 69.2 |
| | 33% | 19% | 24% | 21% | 7% | 20% |
| *AASHTO LRFD 3rd Ed.* | 79.3 | 75.6 | 72.3 | 69.3 | 66.5 | 64.0 |
| | 19% | 7% | 12% | 10% | -1% | 11% |

Note: 1 ksi = 6.89 MPa

**Table 4** – Peak Strain Values for Flexure Tests

| Designation | B-84 | | B-75 | | B-68 | |
|---|---|---|---|---|---|---|
| Top Fiber Strain ($x10^{-6}$ in/in) | -3640 | -2954 | -2614 | -3469 | -3232 | -2630 |
| Average Strain ($x10^{-6}$ in/in) | -3090 | | | | | |

**Table 5** – Comparison of Actual versus Predicted Cracking Load for Flexure Tests

| Designation | B-84 | B-75 | B-68 |
|---|---|---|---|
| Actual Cracking Load (kips) | 18.45 | 19.10 | 19.42 |
| **Predicted Cracking Load Using Predicted Losses** | | | |
| PCI Design Handbook (kips) | 17.21 | 16.65 | 18.03 |
| Moment-Curvature Analysis (kips) | 18.14 | 18.46 | 18.76 |
| Response-2000 (kips) | 16.62 | 17.21 | 17.61 |
| **Predicted Cracking Load (kips) Using Measured Losses** | | | |
| PCI Design Handbook (kips) | 16.66 | 16.85 | 16.54 |
| Moment-Curvature Analysis (kips) | 17.37 | 17.54 | 17.25 |
| Response-2000 (kips) | 15.98 | 16.35 | 16.20 |

Note: 1 kip = 4.45 kN

**Table 6** – Comparison of Actual versus Predicted Ultimate Load

| Designation | B-84 | B-75 | B-68 |
|---|---|---|---|
| Actual Failure Load (kips) | 34.90 | 36.26 | 37.95 |
| **Predicted Failure Load Using Predicted Losses** | | | |
| PCI Design Handbook (kips) | 31.43 | 32.53 | 33.45 |
| Moment-Curvature Analysis (kips) | 32.37 | 33.18 | 33.98 |
| Response-2000 (kips) | 33.86 | 35.06 | 36.09 |
| **Predicted Failure Load (kips) Using Measured Losses** | | | |
| PCI Design Handbook (kips) | 31.10 | 32.07 | 32.67 |
| Moment-Curvature Analysis (kips) | 32.01 | 32.94 | 33.50 |
| Response-2000 (kips) | 33.86 | 34.72 | 35.55 |

Note: 1 kip = 4.45 kN

**Table 7** – Comparison of Actual versus Predicted Shear Capacity (No Stirrups)

| Designation | B-79 | B-72 | B-65 |
|---|---|---|---|
| Shear Failure Load (kips) | 11.70 | 14.91 | 17.89 |
| **Predicted Capacity Using Predicted Losses** | | | |
| PCI Design Handbook (kips) | 15.76 | 16.18 | 16.55 |
| Response-2000 (kips) | 23.28 | 24.26 | 25.20 |
| **Predicted Capacity Using Measured Losses** | | | |
| PCI Design Handbook (kips) | 14.48 | 15.27 | 15.82 |
| Response-2000 (kips) | 21.87 | 23.35 | 24.23 |

Note: 1 kip = 4.45 kN

**Table 8** – Comparison of Actual versus Predicted Shear Capacity (Stirrups)

| **Designation** | **B-79** | **B-72** | **B-65** |
|---|---|---|---|
| Shear Failure Load (kips) | 23.69 | 26.82 | 20.55 |
| **Predicted Capacity Using Predicted Losses** | | | |
| PCI Design Handbook (kips) | 32.26 | 28.55 | 26.45 |
| Response-2000 (kips) | 31.16 | 29.99 | 28.28 |
| **Predicted Capacity Using Measured Losses** | | | |
| PCI Design Handbook (kips) | 30.98 | 27.65 | 24.72 |
| Response-2000 (kips) | 30.65 | 29.72 | 28.50 |

Note: 1 kip = 4.45 kN